Aalto-yliopisto
Aalto-universitetet
Aalto University

Ziya Yektay

Sentinel-2 images for detection of wind damage in forestry

Espoo 30.09.2019
Supervisor: Prof. Minna Rautiainen
Advisors: Dr. Susanne Suvanto
Dr. Mikko Peltoniemi

Aalto University
School of Engineering

Aalto University, P.O. BOX 11000, 00076
AALTO
www.aalto.fi

Abstract of master's thesis

Author Ziya Yektay

Title of thesis Sentinel-2 images for detection of wind damage in forestry

Master programme Geoinformatics **Code** ENG22

Thesis supervisor Miina Rautiainen

Thesis advisor (s) Susanne Suvanto, Mikko Peltoniemi

Date 30.09.2019 **Number of pages** 84 **Language** English

Abstract

Using of Remote sensing for the sake of Earth Observation is getting more and more popular as the number of satellites that are able to measure electromagnetic radiation with a higher spatial, temporal and radiometric resolution is considerably rising. Of all usage of Earth Observation, detection of disturbances caused by natural catastrophe such as wind, earthquake and fire is highly important. On 12th of August 2017, a storm hit South and South East of Finland, bringing harsh disturbances to the forest area in which Pine and Spruce were the main types of land cover. The study area in this region contained land cover types such as Pine, Spruce, Silver birch, and Downy birch. Two sentinel-2 images from 11th of August 2017 and 5th of September 2017 were used to measure spectra behavior of existing features before and after storm in the region. Forest use notifications data and forest-stand dataset were used as ground truth data. For change extraction, univariate image differencing was used using six different indices, namely EVI, NDVI, NDMI, SATVI, TCB, and TCG. Two different approaches were taken for change detection, namely pixelwise and average based, where in the former individual pixels were extracted (from stands) and used for training the models while in the later average of pixels inside each stand was calculated and used for training. Results achieved by average-based showed a better performance in terms of user accuracy and stability than pixelwise approach did.

Keywords Spatial resolution, temporal resolution, radiometric resolution, EVI, NDVI, NDMI, TCB, STVI, TCG, univariate image differencing, Forest use notification

Preface

I would like to thank Professor Aleksi Lehtonen for offering me this exciting Master thesis topic. It was a real pleasure working at LUKE where I was supported and guided by you and other kind and friendly experts. I would like also thank Dr. Mikko Peltoniemi for his support. Especial thanks go for Dr. Susanne Suvanto who supported and guided me so much during the work. Thank you for being so patient, kind and supportive to me. I would like to thank Professor Miina Rautiainen for being my supervisor in this project. The reason why I became interested in remote sensing is because of your great interesting lectures and guides during the courses. Also, your kind constructive comments on the thesis draft at the end of the work was a great guide to me to organize the text in a more logical way. In addition, I would like to thank my wife for being so kind and patient during my 3 years of studies. At last but not least, I would like to thank my parents that have always been there for me and supported me.

Otaniemi, Finland, 30.09.2019

Ziya Yektay

Symbols and abbreviations

BOA	Bottom of Atmosphere
TOA	Top of Atmosphere
OLI	Operational land imager
DEM	Digital elevation model
ISP	Instrument source packet
UTM	Universal Transverse Mercator
VI	Vegetation index
LULC	Land use land cover
NDVI	Normalized difference vegetation index
TCB	Tasseled cap brightness
TCG	Tasseled cap greenness
TCW	Tasseled cap wetness
NDREI	Normalized difference red edge index
EVI	Enhanced vegetation index
SAVI	Soil adjusted total vegetation index
SATVI	Soil adjusted total vegetation index
NDMI	Normalized difference moisture index
UID	Univariate image difference
AI	Artificial intelligence
SVM	Support vector machine
RF	Random forest
RELU	Rectified linear function
PCA	Principal component analysis
PCC	Post classification comparison

LUKE	Natural Resources Institute Finland
GDAL	Geospatial data abstraction library
CSC	ICT solutions for brilliant minds Finland
LTS	Landsat time series
NN	Neural network
NDFI	Normalized Difference Fraction Index
VHSR	Very High Spatial Resolution
OSM	Open street maps
MSI	Moisture stress index
DTM	Digital Train Model
DOS	Dark Object Subtraction
FLAASH	Fast Line-of-Sight Atmospheric Analysis of Spectral Hypercubes
DI	Disturbance Index
FVC	Fractional Vegetation Coverage

1. Introduction.

1.1 Motivation

Huge amount of carbon dioxide is absorbed and converted to oxygen by forests (Dixon et al. 1994). They are considered as the biggest carbon pool mass between our terrestrial ecosystems (Dixon et al. 1994) and changes in this ecosystem are constantly affecting them (Griffiths et al. 2013). Natural phenomenon such as storms and fires are considerably effecting forests structure and their ecosystems (Hobbs and Huenneke 1992) and climate change is one of the side effects of these changes that are occurring in forest ecosystems. (Chen et al. 2013; Eshleman et al. 2009; Tao et al. 2013). Harsh regularly storms cause great windthrow of trees, changes forest structures, and break up the forested landscape. Not only do such damages effect timber industry, wildlife habits, and local economy in a direct way but they also often have long-term impact on forest succession, nutrient cycling, drainage as well as site productivity, therefore, detection of damages in forest is vital for realization of issues such as global biogeochemical cycles, climate changes, and local economy (Wang et al 2009; Einzmaan et al 2016; Guo XY et al 2015).

During the recent years, Finland experienced several harsh storms. In particular, a drastic storm, named Kiira that hit southern of Finland on 12th of August 2017, made gusts of wind up to 32.5 meters per second to the capital city region (YLE 2019). It demonstrated that it was too strong for the Finnish Meteorological Institute's (FMI) measuring devices (YLE 2019). It caused falling of a lot of trees and cut electricity cables in the region (YLE 2019). Figure 1.1 illustrate how powerful the storm was, which managed to fall down a big tree.

Figure 1.1 shows the power of Kiira strom invaded Southern and East of Finland on 12th August 2017 (YLE 2017)

Similarly, on 26th August 2016, another storm, named Rauli, caused a lot of destruction and downed a number of trees causing the cliffs of power lines. Vaasa and Kuopio cities were the ones that were highly affected (YLE 2019).

Considering all disturbances happened in the mentioned cities, a need for a faster and accurate way to automatically detect the location of damaged areas was needed. Not only is automatic detection of disturbances using free-cost-satellite-imagery affordable but it is also safer (not field work required). As a result, fast detection of disturbances prevents more economic and environmental losses that could happen to the damaged forest.

1.2 Thesis Novelty and objectives

This is the first study to examine the usage of Sentinel-2 images with high spatial resolution to detect disturbances caused by winds in forest. As described in literature section, there has been studies in which Landsat imagery with moderate spatial resolution (30 meters) was used for detection of disturbances occurred in forest. However, in this thesis, Sentinel-2 images that offers much better spatial, temporal, and radiometric resolution was examined. Almost all studies took advantage of using individual bands and indices for change detection purposes and then compared their results against one another. However, in this study, the most common bands and indices used for wind damage detection were utilized simultaneously as six independent predictors using two complex models. In addition, a new strategy for removal of clouds was implemented since Sentinel cloud mask was not able to remove all cloudy pixels. The overarching goal of this thesis was to establish an algorithm in order to automatically detect wind damages in forestry using Sentinel-2 images. It also compared performance of two complex models, namely random forest and neural network on detection of wind damages. Furthermore, it gives some recommendations for future studies that are going to work on the same theme.

2. Literature review

In this section the scientific background is reviewed. It explains what has been done so far and the accuracy achieved. Some general background of machine learning is also covered.

2.1 change detection history

Wang et al (2009) compared performance of different change detection methods for detection of disturbances caused by the storm occurred on 29th of August 2005 in forests. Algorithms such as selective principal component analysis (PCA), change vector analysis (CVA), and post classification comparison (PCC) were tried using six different vegetation indices such as RVI, NDVI, SAVI, TCB, TCG, and TCW. The area under study covered Lower Pearl River Valley and neighborhood areas of Washington Parish, Louisiana and states such as Pearl River in Mississippi and Hancock. The area of whole forest in the study areas was about 370000 ha, which included species such as shortleaf pines, longleaf-slash pine, and oak-pine groups (Wear and Greis 2002), blackgum, sweetgum, oak. In terms of climate, the study region enjoyed a humid weather. The geospatial data used in this study contained two sets of Landsat 5 TM images, taken on 22nd of August 2005 and 9th of October 2005, Digital Ortho-photos as well as National Oceanic and Atmospheric Administration (NOAA) aerial photos taken between 30th of August and 8th of September 2005. During the 50-day gap between the obtained images, all damages were assumed to be direct effect of the storm. The Ortho-photos, enjoyed one meter spatial resolution, were mainly used for validation of land cover classification applied on the pre-storm image. The NOAA images were utilized to generate ground truth data. In addition, field surveys were carried out from April to June of 2006 in the region under study. Taking advantage of NOAA photos' interpretations and field works, 6470 pixels that covered an area of 525.36 ha were labeled as damaged forest while 4115 pixels covered an area of 334.13 ha went for undamaged forest. In order to identify land cover classes in the area of study, a combined machine learning technique containing an unsupervised algorithm followed by a supervised algorithm, maximum likelihood in this case, were used. The digital Ortho photos were used to validate the classification process and make sure that only forest areas were chosen by the combined technique. In the next step vegetation indices (VI) were calculated

followed by change feature extraction using algorithms such as UID, selective PCA, and CVA. The study concluded that different change detection algorithms resulted in different range of accuracies. It was also concluded that VI indices played more important roles in comparison with change detection algorithm used in the accuracy achieved. They found indices that took advantage of band 5 and 7 (SWIR1 and SWIR2 of Landsat 5) were able to easily detect areas in which damages occurred. No considerable benefit was discovered using the four different change detection algorithms. However, in terms of reliability, they concluded that UID, CVA, and PCC looked more consistent. At the end, it was suggested that using band 3, 4, 5 on PCC, using TCW and TCB on CVA, and using TCW on UID change detection technique may benefit later studies in detection of disturbances caused by wind in forest.

Vorovencii (2014) studied detection of environmental changes due to windthrows utilizing Landsat imagery. The study area located in Sanmartin forest division in Romainia, which covers an area of 800 ha. The main land cover in this region went for spruce. This study followed three goals, 1- utilizing remote sensing techniques for detection of environmental changes caused by wind, 2- finding the best change detection technique that suited the most for windthrows happened in spruce stands, 3- finding the best threshold values for the used change detection techniques. For satellite data, two images from landsat-7 were used as pre and post images. The first image came from 5th of April 2001 and the second one was taken on 10th of May 2001. In addition to satellite data, orthophoto data was utilized to detect damaged areas. For ground truth, field work was done. The ground truth data contained information about properties of stands hit by storm such as type of trees inside, wood volume affected, slope orientation and their inclination, and type of soil. Three techniques were chosen for change detection, namely univariate image differencing (UID), change vector analysis (CVA), and selective PCA. Speaking of vegetation indices used in this study, SAVI, NDVI, RVI, and Tasseled Cap transformation (TCB, TCW, TCG) were selected. In order to georeference the images, 20 ground control points were used, followed by Dark Object Subtraction (DOS) algorithm to reduce the contribution of atmosphere from the scenes. To remove topographic effects, topographic normalization strategy was applied on the images utilizing a digital train model (DTM). For accuracy evaluation of change detection in this study, 50 stands from each class (damaged and undamaged) were randomly selected, from which error matrix, kappa statistics, and overall accuracy were calculated. It was

concluded that univariate image differencing (UID) performed the best of all (82.3 percent accuracy) when TCW was used. The poorest classification accuracy went for selective PCA using SAVI with 51.3 percent accuracy. It was exposed that TCW was the one that had the most sensitivity for change detection by considering the threshold values smaller than -2s and bigger than +2s, which were standard deviations values calculated from average of pixels inside the disturbed stands.

Guo XY et al., (2015) studied mapping and assessing typhoon-induced forest disturbance in Changbai Mountain national nature reserve. It focuses on assessment of the extent of damages caused by a Typhoon Vera happened on 28 of August 1986. Speaking about the area under the study, Changbai Mountain National Nature Reserve is an area that is situated between North Korea and China. It covered an area of 1965.38 km^2. The area enjoyed variety range of topography from 800 meter to 2700 meter above sea level. In terms of land cover, depending on the different topography in the region there were mainly three types of forest, namely the forest populated by Rhododendron L., and Vaccinium Linn located in areas that were above 2000 meter from sea level, brich forest that were between 1700 and 2000 meter above sea level, and the forest dominated by Abies nephrolepis, Picea koreana, and Picea jezoensis trees located in areas with elevation less than 1100 meter above sea level. United Ntiones appointed Changbai Mountain National Nature Reserve as a Biosphere Reseve in 1979 (Shao et al. 1996), therefore, the study area was watched by United Nations for about 50 years, meaning that human activities were highly restricted, so any changes in the region was assumed to be from natural damages. The main goals of this study were 1- make an estimation of damage severity 2- evaluate how much topography of the region can contribute to the intensity of disturbances in forest 3- examine recovery actions taken after the storm from 1987 to 2010. In total, 13 cloud-free Landsat images taken between 1985 and 2010 were utilized in this study. Middle of May to early August were the time span all images were selected, which was a growing season in the region. For geo-referencing of the scenes, 25 ground control points were used. Fast Line-of-Sight Atmospheric Analysis of Spectral Hypercubes (FLAASH) radiative transfer algorithm was applied on the selected images to reduce the effect of atmosphere (Adler-Golden et al. 1998). In addition to satellite imagery, digital train model was created using Advanced Space borne Thermal Emission and Reflection Radiometer (ASTER) data. This data mainly was used for creation of slope and train aspect in the region of study.

Furthermore, for ground truth data, field work was carried out to create a map (called reference map) that illustrate disturbed areas in the region. Climate data was also used in this study to examine possible correlation between climate changes and forest recovery. One extra landsat-5 image taken on 14th May 1985 (pre-storm) was utilized to help understanding of existing land cover in the region and create a non-forest mask used to differentiate forest areas from other land covers. Ten different classes were generated based on this image using a software named ENVI, which took advantage of Maximum likelihood classifier algorithm to make the classification. The classes were as following 1-snow cover 2-water body 3-bare land 4-meadow 5-mountain birch forest 6-evergreen coniferous forest 7-mixed forest 8-larch forest 9-hard wood forest and 10-construction land. For damage detection, the disturbance index (DI) was used following the non-forest mask applied to exclude non-forest areas, meaning that only pixels labeled as Mountain Birch Forest, Larch Forest, Evergreen Coniferous, Mixed Forest, and Hardwood Forest were taken into DI calculations. For change extraction, Image difference were calculated, meaning that DI of 1985 was subtracted from DI of 1987. High dDI values (post-DI – pre-DI) were regarded as indication of damaged areas while negative and zero went for growing forest and healthy forest respectively. For evaluation of the achieved accuracy during damage extraction, the reference map was overlaid with dDI image. Visual inspection was taken to assess the degree of similarity between the reference map and dDI image. The results showed a high degree of consistency in the two images even though there were also areas that overestimation of windthrow occurred. The factors that was considered to be contributing to this difference was assumed to be from the ground survey data due to terrain that were hard to access, different surveyors may have had different inference of the scenes, and overlooking of areas with small disturbances. The results showed some particular topography in the region contributed to the disturbances caused by the storm. For instance, Over 98 percent of windthrow was reported in the areas with height of 2000 meter above sea level. Regarding forest recovery actions taken after the storm, the results represented dynamic recovery process. During the first few years after the storm, there was a constant growth in the value of DI due to policies taken by forest center, meaning that clear-cutting was applied to the disturbed areas, which caused a big decrease in the value of DI. DI values started to diminish after coniferous trees species were planted by forest owners in the following years. Overall, this study concluded that DI

algorithm could be considered as an effective method for forest damage detection caused by winds.

Grybas et al., (2015) studied the effect of wind on land cover in Assateague Island National Seashore with 60 km long situated in United States of America. The main goal of study was to examine land cover changes caused by a storm occurred in October 2012 in the Island. Two different change detection algorithms were tried namely pixel-based and object-based approaches using random forest classifier. For change extraction, univariate image differencing (UID) was used. The scenes obtained for this study were from Landsat-8 (post-images) and Landsat-5 (pre-images), which were two series of images (multi temporal) were download from 2011 and 2013. Finding suitable imagery (clear sky) was a challenge reported in this study. Vegetation indices generated for this study were NDVI, moisture stress index (MSI), TCB, TCG, and TCW since it was suggested to perform well by the previous studies. The ground truth data was generated by the help of NOAA C-CAP classification scheme, resulting in 10 different land cover features, namely agriculture, deciduous forest, developed, estuarine, evergreen forest, mixed forest, open water, palustrine, shrub, and unconsolidated shore. For each land cover, about 100 samples were measured, which was then verified by high resolution imagery generated by National Agricultural Inventory program imagery, Google Earth, and field assessments. In the next step, 50 sample from each land cover was used for training the model (RF) and the rest was used for testing of the classifier, which was followed by several classifications of pre and post storm images. Next, UID was applied to extract possible changes from the images. For segmentation, the multi-resolution segmentation algorithm was applied on NDVI image difference to segment the image. At the end, It was concluded that there was no difference between accuracy achieved by pixel-based and object-based. UID detected less area as change compared to PCC and the reason was that PCC was suffering from slivers effects, the same features' geometries in different images varies, which caused misclassification of areas left at the edge of features.

Einzmann et al (2017) that studied monitoring of forest disturbances caused by storms in forest introduced a change detection technique that was implemented in two separate steps using very high-resolution imagery provided by Rapid Eye Platform. In the first step, to detect windthrow areas that are bigger than 0.5 ha, an object-based bi-temporal change technique analysis was used. To implement this, a

Random Forest model, a semi-automatic feature extraction technique, and a large-scale average shift algorithm (for image segmentation) were used. Vegetation indices, spectral transformation, spectral behavior, and texture were utilized as inputs to the model. In the second step, to detect small fallen trees, a hybrid-change detection strategy was implemented, which combined the features that were more important in the last processing step with Multivariate Alteration Detection and Spectral Angle Mapper. To validate the results, field data that was generated by on-site presence was used. In addition, orthophoto of sites under study helped for further validation of the study. Vegetation indices that were used for the study were Atmospherically Resistant Vegetation Index (ARVI), Difference-Difference Vegetation Index (DD), Difference Vegetation Index (DVI), Enhanced Vegetation Index (EVI), Green Atmospherically Resistant Vegetation Index (GARI), Green Normalized Difference Vegetation Index (GNDVI), Infrared Percentage Vegetation Index (IPVI), 2nd Modified Soil Adjusted Vegetation Index (MSAVI2), Normalized Difference Red Edge Index (NDREI), Normalized Difference Greenness Index (NDGI), Normalized Difference Red Edge Blue Index (NDREG-B), Normalized Difference Vegetation Index (NDVI), Normalized Near Infrared (NNIR), Plant Senescence Reflectance Index (PSRI), Red Edge Normalized Difference Vegetation Index (REG NDVI), Red Edge Ration Index 1 (RRI1), Ration vegetation Index (RVI), and Soil Adjusted Vegetation Index (SAVI). They concluded that using random forest performed very well considering comparing its results with validation data and it was recommended for future studies to take advantage of RF classifier if windthrow detection is the goal of study. Of all indices that were used, they found that indices that enjoyed the use of red edge and blue bands such as PSRI, NDREDI played the most important role in detection of disturbances. Sentinel-2 usage also was recommended for future studies since it had the main requirement bands, namely three red edge, and short infrared bands.

Wang et al (2018) studied vegetation disturbances caused by storm in Xiamen Island, China. The paper assessed the effect of a storm occurred on September 15th, 2016, taking advantage of two high spatial resolution satellite images. The main goals of this study were to examine the vegetation disturbances and to determine type of vegetation species, trees, shrubs and grasslands, that were effected the most by the storm. The study area was located in south of Fujian Province in China with

an area of 145.6 km2 and elevation of 339.6 meter above sea level. The island was known as the center of Xiamen city, meaning that the type of vegetation in the study area enjoyed regular urban vegetation features. Speaking of existing tree species, Acacia confuse, Delonix regia, Bauhinia variegate, Chorisia speciosa, Ficus benjamina, and F. concinna were the dominant type trees in the region under study. Storms were common natural events in the region hitting at least five times a year, which usually happened between July and September. Two high spatial resolution images from Ziyuan-3 and Gaofen-2 (Chinese civilian high-resolution platforms) were chosen for damage detection analysis. The pre-image was taken by ZY-3 on forth of February 2016 while the post-image was captured by GF-2 on twentieth of September 2016. This gap between two images was due to lack of qualified images before and after storm, which was noted as the most common issue when one was interested in finding images in rainy and cloudy weather. One important difficulty of using high spatial imagery was the lack of proper NDVI seasonal data, which is still an issue to consider when high resolution scenes are chosen. This data (seasonality data) generated by moderate imagery platforms named MODIS and NOAA meant for distinguishing and removing seasonality effects from the images, meaning that one can use this NDVI data (representing the seasonality effects) to remove seasonality interference and focus only on non-seasonal damages. There was no such useful data for high spatial resolution images in order to calibrate the selected images. This is due the fact that temporal resolution was relatively low for higher spatial resolution imagery. In addition, dense clouds in the existing images made it worse, therefore, addressing vegetation seasonal interference plays a critical role in the final accuracy of such studies. In order to determine seasonality effect and remove it from the images in this study, 3 extra Landsat 8 OLI images taken on first of January 2016, fifth of March 2016 and thirteenth of September 2016 were acquired. Furthermore, another image from Landsat 8 OLI taken on third of January 2017 was obtained to examine regeneration of vegetation 5 month after the storm. Radiometric and geometric correction as well as image fusion were applied to the images in image pre-processing step followed by geo-referencing of the images using ground control points. A quadratic polynomial algorithm was applied to avoid image distortion during resampling followed by atmospheric correction of the images using Chavez model. To implement the image fusion on the ZY-3's 6-meter bands and convert them to 2-meter bands, pan-sharpening technique was utilized. The same approach was used on GF-2 image to improve its spatial resolution from

4-meter to 1-meter. In the next step, to make two images consistent in terms of their spatial resolution, nearest neighbor technique was used to resample GF-2 bands to 2-meter resolution. NDVI index and fractional vegetation coverage (FVC) were calculated for both images. In order to calculate FVC, the Carlson and Ripley's (1997) model was chosen over the other existing model named Gutman and Ignatov's (1998) model. The reason for selection of Carlson and Ripley's algorithm was that the study area enjoyed low rate of vegetation cover. Gutman and Ignatov's was recommended for areas with high rate of vegetation cover, meaning that choosing the right model depended on density of vegetation coverage in the study areas (Jiang et al. 2006; Xu et al. 2013). For the classification of vegetation in the study region, support vector machine (SVM) was used since it was known to perform well when it comes to classification of heterogeneous urban areas (Mountrakis et al. 2011). The other reason for choosing SVM over the other shallow models was the fact that size of training datasets could not affect its performance (Linden et al. 2007; Mountrakis et al. 2011; Tigges et al. 2013). Trees, shrubs and grasslands were the main land cover types selected for the classification. For training data, Google Earth high-resolution images were used to extract training samples for each land cover class from the images. In order to apply seasonal variation correction and eliminate its effects, three moderate resolution images from Landsat 8 OLI were obtained since there was no qualified high resolution images available (no free cloud images). The first image was from first of January 2016, the second image came from fifth of March 2016 and the third one was from thirteenth of September 2016 (2 days before the storm). It is worth mentioning that if there had been qualified high spectral imagery available, two images from February and September 2016 would have been enough. The reason for using three moderate images was that there was also no free cloud image for Landsat 8 OLI in February, therefore, an average of February and March imagery was used to simulate the not existing February image. NDVI values were calculated for both images, the simulated February one and September image followed by a sampling criteria, a 3×3 grid, to sample pixels throughout the study area. Next, a polynomial regression model was established to determine the relationship between the two images, which then was used to eliminate to seasonality variation interference from the two high spatial resolution images. For damage detection, image difference between NDVI and FVC were calculated (after image – before image) for the whole study region. The overall change extraction accuracy reported for this study was about 91 percent. The

accuracy of results was validated by comparing the achieved results with random samples extracted from the original pan-sharpened high spatial resolution images, which was a technique recommended by Schneider (2012). To Discover the types of species that were affected the most by the storm, 7 areas that had the highest value of NDVI difference were chosen in the study region. Baidu Total View, Chinese version of Google Street View, was used for identification of type of trees in the 7 selected regions. It was exposed that the most affected land cover was trees, which in the area of the study were mostly as following Acancia confuse, Delonix regia, Bauhinia variegate, Chorisia speciose, Ficus benjamina and F.concinna trees

Stych et al., (2019) evaluated the impact of wind and bark beetle damages on forest using the time series of Landsat data in two different parks in Slovakia and Czechia. The area of study in Slovakia was about 73 square km that was mostly covered by spruce forest while in Czechia it was about 900 square km in which spruce forest dominated the whole area. The time span of the study was 23 years from1992 to 2015. Depending on the type of forest in ten different localities in these two parks, ten different vegetation indices, namely NDMI, FMI, NDVI, SR, TVI, WNDII were selected. Regarding satellite data, eleven images were chosen for this study. It was mentioned that crucial steps in this study were finding clear images and selection of sensing date of the images. It was recommended that the most suitable time for evaluation of vegetation in forest was from the summer to early autumn due to seasonality effects on the spectra of land covers. For validation of analysis, data from field survey was used. This data contained information about forest management plans, field records made by foresters and nature conservation data. In order to make the images compatible and comparable to one another, radiometric normalization technique was used, which removed the effect different sensors, different sensing date of images, and phenology issues. Results stated that different type of damages (whether it was biotic or abiotic) had different effects on the health of vegetation. At the end, it was concluded that indices that take advantage of RED, NIR, and SWIR bands such as NDMI and WNDII could be more sensitive and effective for detection of wind disturbances in forest.

2.2 Vegetation indices

1- NDVI

Plants produce sugar and oxygen during a process called photosynthesis in which water, light and carbon dioxide are consumed. The reason why healthy plants are green is the existence of chlorophyll that highly absorbs visible light while reflects near infrared light. Considering the mentioned facts, one may use these lights and their combinations to study the behavior of vegetation in areas of interest. Of all vegetation indices, NDVI is the most prominent index used to study spectra behavior of vegetation (Wang et al., 2009).

NDVI index can be calculated using formula 1:

$$NDVI = \frac{(NIR - RED)}{(NIR + RED)} \qquad (1)$$

2- Tasseled Cap Transformations

One of the common techniques when using remote sensing data is to use ratio and combination of bands. Tasseled Cap Transformation is an axis reduction strategy in which data points are projected to a new space with often less number of axis that are in direction of highest variance. In literature, reducing dimensionality of data points is called principal components analysis. In other words, it extracts another representation of the data, which is not clear for users. The first axis is meant for representing brightness (TCB), which mostly represents soil, concrete, rocks and man-made materials. TCG (greenness) is the second axis that mostly expose the behavior of vegetation while TCW (wetness) is more focused on water and soil (Wang et al., 2008).

3- Normalized Difference Red Edge (NDREI)

This index is sensitive to three factors namely chlorophyll content that is inside plants, changes in green mass and soil effects. High value of NDREI means that there is higher level of chlorophyll content inside leaves while lowest values could be due to existence of soil (Einzmann et al., 2017).

NDREI would be a more accurate measure of how healthy vegetation is when there is high level of chlorophyll inside leaves. This is because red-edge radiation

is semi-transparent to leaves than red light, therefore, it would be less likely to be absorbed completely by canopies. As a result, NDREI could be a better choice for intensive management applications throughout the growing season than NDVI that can't perform well when there is a lot of accumulated vegetation and high level of chlorophyll content in leaves (Paulina Raeva et al. 2018).

NDREI can be calculated using formula 2:

$$NDREI = \frac{NIR - REG}{NIR + REG} \qquad (2)$$

where NIR stands for near infrared region of electromagnetic radiation (EMR) while REG goes for visible read edge part of EMR. Read edge is regarded as the turning point where vegetation changes its spectral behavior.

4- Enhanced Vegetation Index (EVI)

EVI is another vegetation index that is highly recommended for areas in which the mass of vegetation is high. This index uses a combination of near infrared, red, and blue bands, which meant for addressing the issue of atmosphere and soil effects on NDVI values. In other words, it is able to lower the effect of atmosphere and rectify upcoming radiation caused canopy background. Formula 3 shows how EVI can be calculated (Xue et al., 2017).

$$EVI = 2.5 \times \frac{(NIR - RED)}{(NIR + C_1 \times RED - C_2 \times BLUE + L)} \qquad (3)$$

In which RED and BLUE stand for visible red and blue parts of EMR while NIR goes for near infrared region of electromagnetic radiation.

Considering formula 3, there are two coefficients, named, C_1 and C_2 ,that are responsible for rectifying the effect of atmosphere while L is aimed to target soil background. The standard EVI parameter values are 1, 6, and 7.5 for L , C_1 , and C_2 respectively (Xue et al., 2017)

5- Soil-Adjusted Total Vegetation Index (SATVI)

This index can measure dead and photosynthesizing vegetation. The usage of short wave infrared has made this index less common compared to the others mentioned. SATVI is well known when mapping surface conditions, plant litter, photosynthesizing biomass, and measuring aboveground biomass is the interest of studies. It makes use of SWIR1, SWIR2, and RED that are available for Sentinel, Landsat, MODIS, and ASTER. The recommended value for L is 0.5, which corresponds to the soil-line slope (Torbick et al., 2016; Marsett et al., 2006).

$$SATVI = \frac{SWIR1 - RED}{SWIR1 + RED + L} \times (1 + L) - \frac{SWIR2}{2} \qquad (4)$$

In which SWIR1 and SWIR2 go for non-visible short wave infrared parts of EMR while RED stands for visible red region of electromagnetic radiation.

6- Normalized Difference Moisture Index (NDMI)

Changes in the water content of vegetation can be estimated by this index that take advantage of SWIR and NIR bands. Due to high sensitivity of NDMI to changes in water content of leaves, this index may be efficient for usages such as damage detection, watching drought and estimating yield depletion (Hadi et al., 2018; Schultz et al., 2016).

Formula 5 illustrates how NDMI can be calculated:

$$NDMI = \frac{(NIR - SWIR)}{(NIR + SWIR)} \qquad (5)$$

Where SWIR and NIR stand for short wave infrared and near infrared parts of electromagnetic radiation respectively.

Values that are bigger than 0.5 are considered as water bodies while vegetation gets much smaller values, making recognition of water bodies from vegetation much simpler. However, man-made features are assigned values that are less than 0.2 (Stych et al., 2019)

2.3 Machine learning

2.3.1 Definition and history

Giuseppe in his book defines machine learning as “an engineering approach that gives maximum importance to every technique that increases or improves the propensity for changing adaptively” (Bonaccorso, 2018).

“The purpose of a machine learning model is to approximate an unknown function that associates input elements to output ones” (Bonaccorso, 2018)

Models in machine learning are trained rather than explicitly hard coded. Models are exposed with a lot of examples that are associated to a task, then, they try to determine statistical pattern existing in the given examples, ending up with a set up rules that can automate the task. An example for this could be labeling images that illustrate numbers from one to nine (each image represents one particular number). A machine-learning system should be presented many examples that are labeled by us, and then the system starts learning existing statistical patterns based on relating each picture to its label (Chollet, 2018).

Machine learning started to gain popularity in the 1990s. since then, it has earned a lot of attention as a sub category of artificial intelligence (AI).

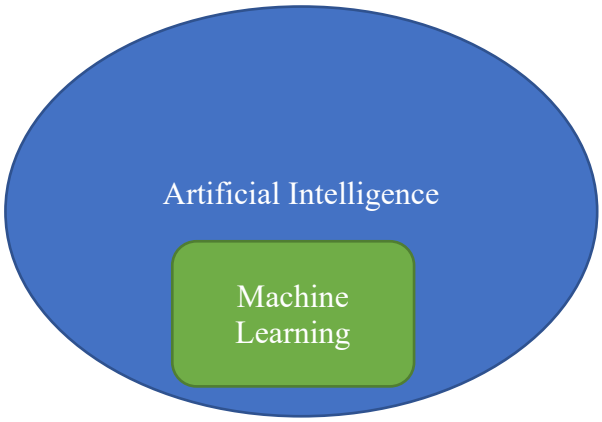

Figure 2.1 shows the relation between AI and machine learning (Chollet,2018).

2.3.2 Shallow learning Vs Deep learning

To describe the difference between deep models and shallow ones, it should be clarified what they do. Three different steps are needed before thinking about establishing a model:

1. **Input data**: depending on the task, input data can be different. Supposing one aims to classify pixels in an image, the input data could be a series of images (Chollet, 2018).

2. **Examples of expected results:** depending on the task, results vary. Supposing that input data is an image, the output data could be labels, a set of meaning full numbers defined in training step, that are assigned to pixels (Chollet, 2018).

3. **Monitoring technique:** This is an important step since it defines the learning part of the algorithm, meaning that it measures the difference between a model's current output and ones that are expected. The magnitude of difference is used in the next step to correct weights assigned to each node (Chollet, 2018).

A role of a machine-learning algorithm is to transform data imported as input to results that are meaningful, which is a procedure that is achieved by exposing known sample data and their associated outputs, therefore, one may say that the main issue in machine learning is transformation of input data into another representation that is more beneficial for classification. By representation here, the author means different way of looking at data, which makes us closer to the expected output. For example, a colorful image can be represented in two different ways namely RGB, stands for red, green, blue, or HSV, goes for hue, saturation and value. These are regarded as two different representations that can be used for the same data in hand. Considering these representations, doing tasks may be harder with one while it becomes easier with the other one. For instance, selecting all green pixels in an image is much simpler with RGB format while making the image less saturated would be easier with the other one (HSV). Machine-learning algorithms' job is to find good representations for the input

data. In other words, they transform the data to make it more reactive to the tasks (Chollet, 2018).

Machine-learning models' jobs is to automatically discover transformations that reform the input data into more-helpful representations for given tasks. These operations range from changing coordinates or linear projections to non-linear operations. Machine-learning models are not typically considered smart in discovering transformation, therefore, they just look into some pre-made group of operations, which is so called hypothesis space. As a result, looking for the best representation of data inside a predetermined space, and taking advantage of signal from loss function in order to learn is the main role of machine learning algorithms (Chollet, 2018).

Deep learning is considered a sub category of machine learning. It offers a new way in which consecutive layers are formed. The deep word stands for the idea of having consecutive layers that have different representation of input data. Cutting-edge deep learning models usually contains hundreds of consecutive layers of representations and they are learnt spontaneously from exposure to training set of data in hand. However, shallow models focus on either one or two transformation of the input data, which is already predefined in their hypothesis space. That is why they are called shallow models since their hypothesis space is limited (Chollet, 2018).

2.3.3 Branches of machine learning

1. **Supervised learning:** This type of learning is definitely the most common branch of machine learning these days based on a research done by Kaggle.com. It includes associating input data to targets (or labels) that are already known to us, which is so-called learning. These labels are usually handled by humans. Nowadays, most application are benefiting from this type of machine learning to meet their needs (Chollet, 2018).

Decision trees:

They follow a structure that is similar to a flowchart, which allows for classification of dataset imported as input. Decision trees are straightforward to interpret and visualize. Decision trees are regarded as shallow models (Chollet, 2018).

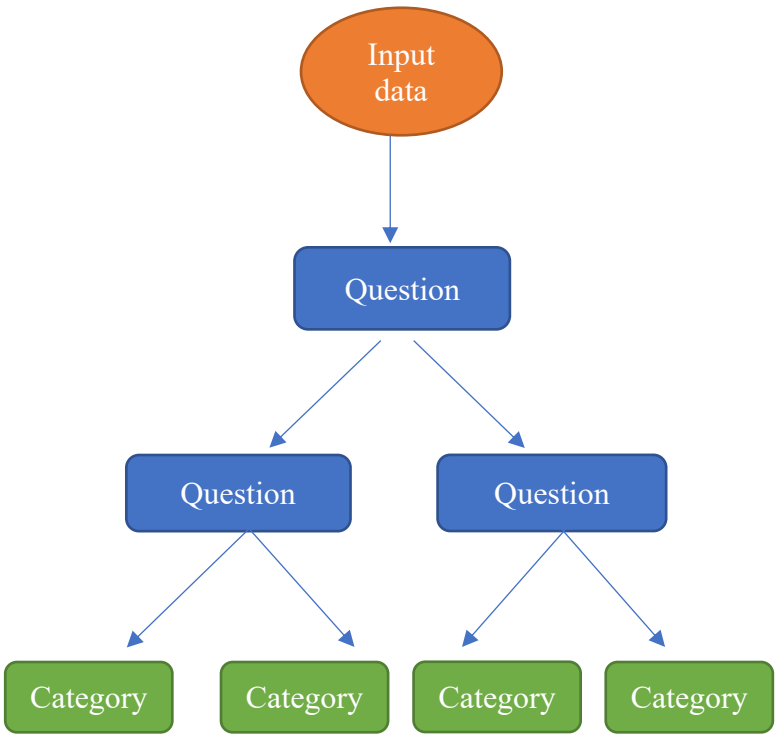

Figure 2.2- A decision tree: the parameters that are learnt are the questions about the data (chollet, 2018)

Decision trees can be used for both regression and classification problems. A classification tree is similar to regression tree. The only difference is that a classifier tree is able to make prediction for categorical data, which outputs discrete values (finite labels) while regressor tree generates continues output (infinite) (James et al., 2015).

In order to estimate how well the classifier tree performs, either Gini index or cross-entropy can be calculated. Formula 6 represents how Gini is calculated:

$$G = \sum_{k=1}^{k} p_{mk}(1 - p_{mk}) \qquad (6)$$

In this equation p_{mk} shows frequency of observation in the m_{th} part that comes from the k_{th} class.

Cross-entropy can be calculated via formula 7:

$$D = -\sum_{k=1}^{k} p_{mk} \log p_{mk} \qquad (7)$$

In other words, one may use Gini or Entropy to find the best split for a model, which is the crucial part of creating a successful model (James et al., 2015).

The problem with this model is that one can't usually get the best user accuracy that could be achieved by other type of models such as ensemble ones. High variance is one of the reasons for this, meaning that various splits in the data used for training would generate trees that are not similar to each other (Bonaccorso, 2018).

Random forest:

Random forest is one of the shallow models that has gained so much popularity between supervised models. It generates a forest and makes it random. The forest data that it creates is an average of best trees trained with a technique called bagging (Bonaccorso, 2018).

The main idea in bagging (aggregating) is to get an average of many noisy but approximately unbiased tree models, and therefore lower the variance. Trees could be good candidates for bagging since they can extract complex interaction structures (patterns) that might exist in the data and if grown deep enough, they will have a relatively low bias. because trees are usually noisy, an average of them could benefit us (Hastie et al., 2008).

In practice, to enhance performance of single decision trees, one may use many trees with a set of features that are chosen randomly, which is the core idea behind random forest. The workflow is that features are chosen haphazardly for each tree and for each split. By randomly dropping out candidate features from each split, random forest decorrelates the trees that are highly correlated (due to existence of particular features that could perfectly classify a certain class). For classification problems, the value split is typically chosen to be square root of attributes in the dataset (Hastie et al, 2008). Another nice benefit of this model is that it could be used for both regression and classification problems.

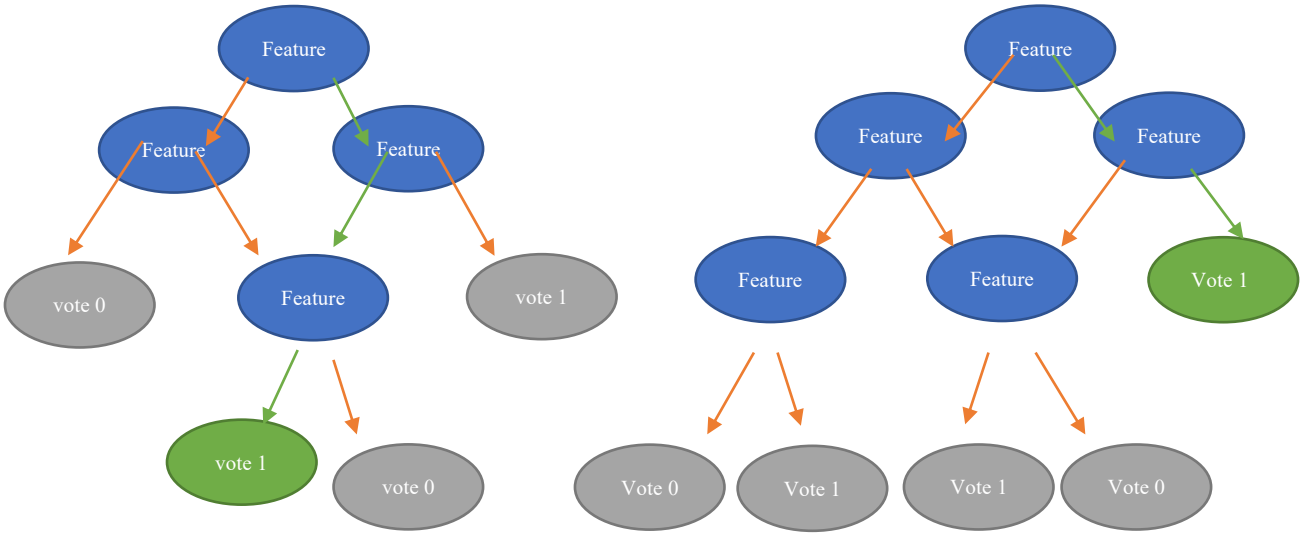

Figure 2.3-small forest voting for class 1 (chollet, 2018)

Figure 2.3 shows a small forest that contains two trees. Supposing that trees features are some bands for each pixel, random forest is voting for class 1.

Neural Network:

In deep learning, stack of layers are formed via models named neural network. These layers are different representation of data imported as input.

Deep learning is regarded as a mathematical frame work where representations of data are learnt (Chollet, 2018).

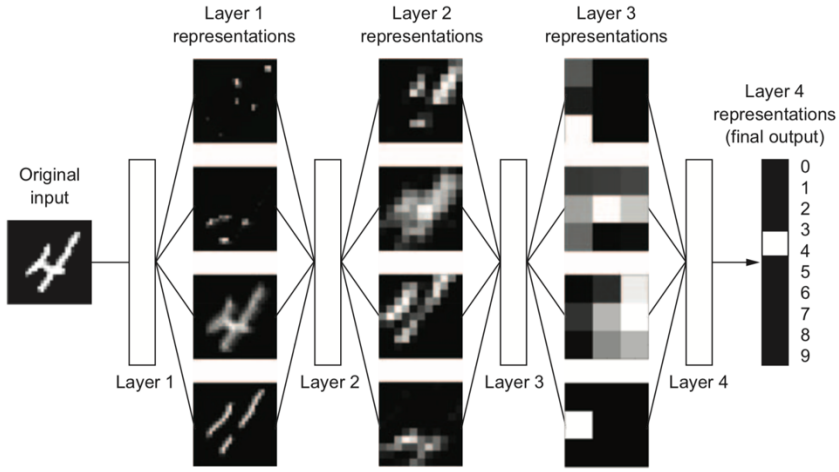

Figure 2.4- a neural network (Chollet, 2018)

Figure 2.4 illustrates how a network is able to transform a digital image to representations that are not similar to the input image. In fact, in each layer (or representation) part of image may be taken into account and the deeper the layer is, the more refined information will be (Chollet, 2018).

In a neural network, NN, the main goal is to make use of score achieved by loss function to improve the weights in a way that minimize the loss score for the current input (Chollet, 2018).

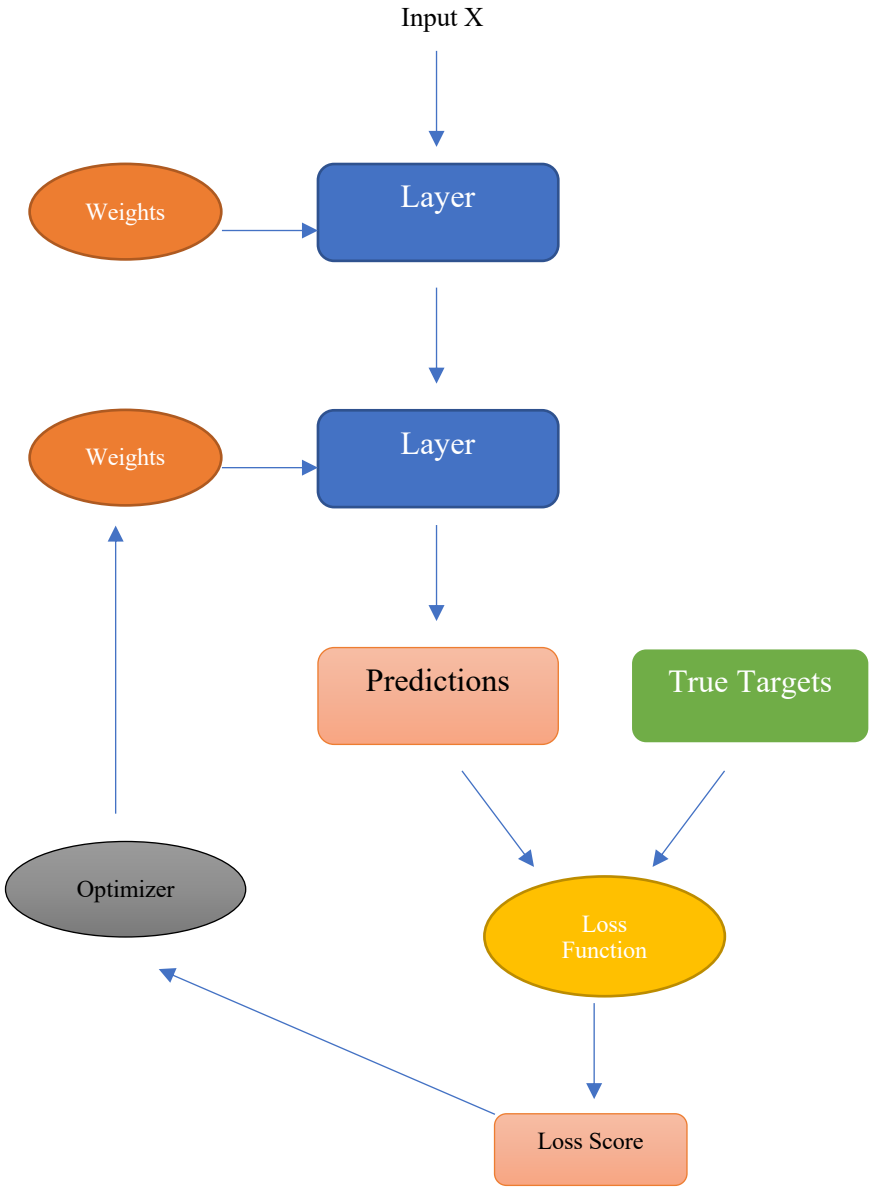

Figure 2.5- shows the main structure of a neural network (Chollet, 2018)

Figure 2.5 shows the whole structure of NN.

To have a richer hypothesis space with which we could take advantage of deep layers, non-linearity, activation functions, are needed. One of the most common activation functions in deep learning is called Relu. However, there are many others that could be considered as building a deep network such as Elu, Prelu and so on (Chollet, 2018).

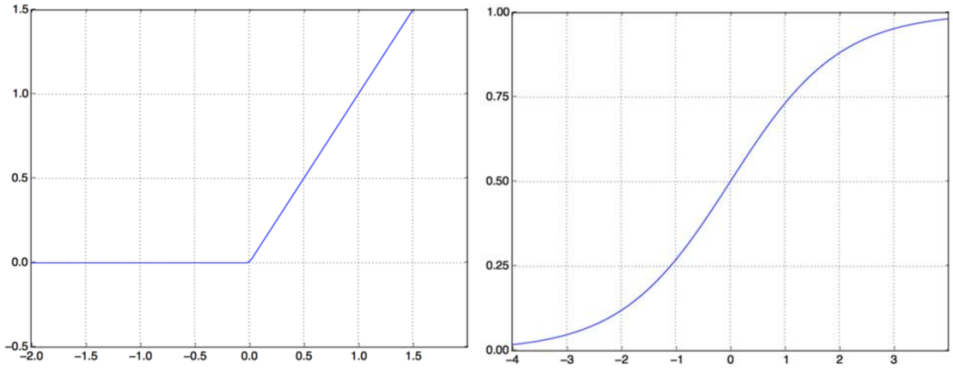

Figure 2.6-left figure represents a rectified linear function (RELU) while the right one shows a Sigmoid function (Chollet, 2018)

2. **Unsupervised learning:** This type focuses on discovering patterns that are not often clear for humans without using any labels. It is usually used for verity of purposes such as noise removal, visualization of data. This type of machine leaning is mostly used to get a better understanding of data in hand before trying any supervised algorithms. Of all categories present in this branch of machine learning, clustering technique and dimensionality reduction are well-known categories of unsupervised learning (Chollet, 2018).

K-means:

When k-means algorithm starts working, it randomly selects centroids in the dataset space, which would be the initial centroids assigned to every cluster, then iterative calculations begin in order to optimize the location of the centroids (Chollet, 2018).

The process could be stopped when one of following conditions is met:

1. The centroids do not change any more (stabilized).
2. The algorithm reaches the number defined for maximum iteration, this number can be set by users (Chollet, 2018).

The workflow taken to implement k-means is described below:

1- Data assignment step:

Once initial random centroids are defined, every point in the dataset finds new centroid that is the nearest through calculation of the squared Euclidean distance. Assuming c_i is a centroid in a set of centroids C, every individual observation is associated to one cluster using the following formula (Chollet, 2018):

$$argmin\ dist(c_i, x)^2 \qquad (8)$$

Where dist(.) is considered as the standard Euclidian distance. It is also assumed that the group of sample points for each i^{th} center of cluster is s_i.

2- updating centroid position step:
During this phase, the centers of all clusters are recalculated. It is done by formula number 9:

$$c_i = \frac{1}{|s_i|}\sum_{x_i \in s_i} x_i \qquad (9)$$

The algorithm keeps iterating between these steps until one of stopping criteria is met (Chollet, 2018).

2.3.4 Overfitting and underfitting

The main difficulty as implementing a machine learning algorithm is relation between generalization and optimization. The former is about how well a model that is trained predict on unseen data while the latter is about how to adjust a model to achieve the best accuracy possible using training data (Chollet, 2018).

The act of fighting overfitting issue is named regularization. In the following lines, dropout technique is briefly explained (Chollet, 2018):

1- Dropout: This is the most common way of dealing with overfitting used in neural networks. When dropout is implemented on a layer, in a random way it drops some of output features by setting them as zeros. For instance, if the given layer normally outputs a vector like [0.3, 0.7, 2.8, 8.2, 3.1], it will change it to something similar to [0, 0.7, 2.8, 0, 3.1] depending on dropout rate, which determine how many elements should be zeroed (Chollet, 2018).

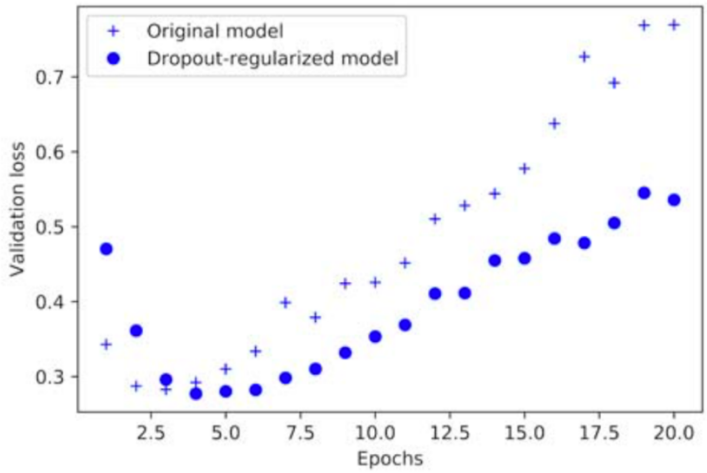

Figure 2.7 represents the effect of dropout on validation loss (chollet, 2018)

2.3.5 Evaluating machine-learning models

Evaluating a model need to divide the data in hand into three sets namely training, validation, and test. A model is trained using training data and then evaluated via validation set. In order to evaluate how well a model performs, test data is applied. The reason for this is that developing a machine learning algorithm always require tuning its parameters and configuration. Considering RF as an example, one can change the way the model is formed via parameters such as min_sample_split or n_estimators where in the former the minimum, one can set how many samples is needed to split a node and in the latest the number of trees in the forest is set (Chollet, 2018).
There are two common cross validation techniques namely Simple Hold-Out Validation and K-Fold Validation.

1- Simple Hold-out technique
   In this method, a dataset is divided into two parts namely training set and validation set. A model is trained using training data followed by testing of the model using test data.

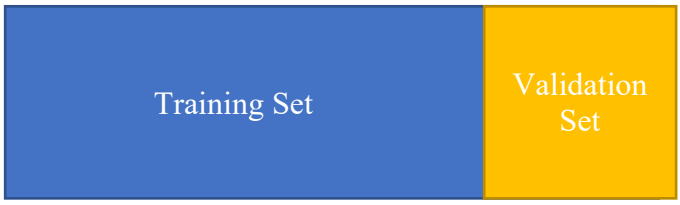

Figure 2.8 shows simple hold-out validation technique (Chollet, 2018)

2- K-Fold Validation

This method is used to train and validate the models. Considering this approach, a dataset is split into K equally sized partitions. Models are trained using K-1 partitions, and evaluated using the remaining partition. As a result, final accuracy can be calculated by taking scores achieved in K-1 steps (Chollet, 2018).

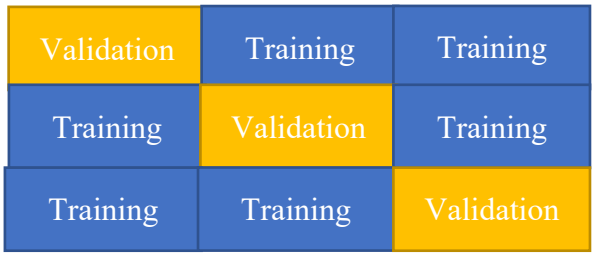

Figure 2.9 shows three-fold validation (Chollet, 2018)

2.3.6 Class balancing

One of the important factors that should be kept in mind as using machine learning models is that one should make sure that training dataset is balanced, meaning that the number of observations in classes should be almost even. This is because of the fact that we would want models care about all possible classes existing in the dataset in a fair way otherwise we would get a biased decision towards one particular class that has probably the highest rate of samples in the dataset (Bonaccorso, 2018).

Imbalanced dataset refers to conditions in which frequency of observations is not the same for all classes in a classification dataset. Machine learning models such as random forest can't perform well when training data is imbalanced. In other words, random forest would tend to voter for classes with the biggest frequency, which is called majority class (biased decision). This issue may get even worse when one is interested in a precise classification of a rare class in a dataset, which is called minority class (Chollet, 2018).

3. Methodology

3.1 Study Area

The study area in this thesis covered a geographic region between (25.131, 61.321), (27.182, 61.334), (27.176, 60.348), and (25.187, 60.336) shown in Figure 3.1. Scots pine and Norway spruce are the most common types of trees found in this area. In addition to timber production, this forest may provide recreation opportunities, which makes it valuable to the environmental well-being and local economy. On 12th of August 2017, a drastic storm, named Kiira, invaded this region and caused damages to the forest.

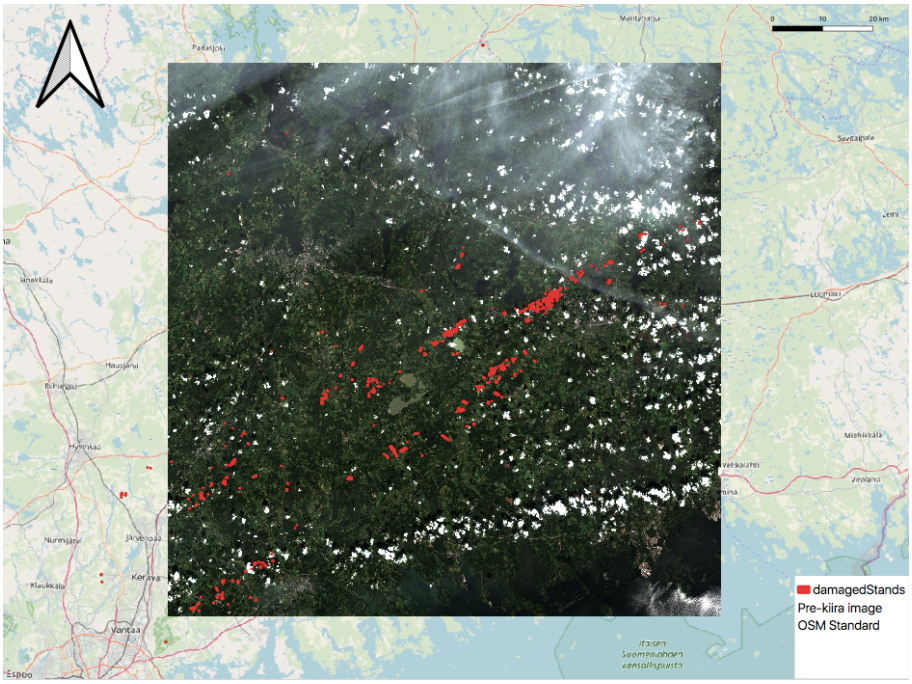

Figure 3.1 shows the extent of study area

Figure 3.1 shows the extent of the area under study and distribution of stands that experienced damages.

The extent of this study covered an area offered of 100 km by 100 km, which also can be seen from Figure 3.1. The type of forest in this region is shown in table 2. The metadata that was used for the estimation of forest type in the region is available from links [8] and [9]. These data came from Forest Center in Finland, which had an

attribute called “declarationdevelopmentclass”. Table 1 shows some of the metadata about the stands:

Table 1 shows code explanations used to estimate age of forest in the study area

Label	Description
1	Open land
2	Seed-tree stands
3	Recently planted forest under 1,3 m
4	Recently planted forest over 1,3 m
5	Recently planted forest with hold-over trees
6	Young growing forest
7	Grown up growing forest
8	Mature forest
9	Shelter wood forest
10	Poorly productive forest
11	Uneven-aged forest

Table 2 illustrated the land cover type in the area of study. As can be seen, the majority part of forest in this region contained growing forest and mature forest.

Table 2 shows proportion of different land cover in the study region

Land cover type	Percentage
Open land	0.55
Seed-tree stands	0
Recently planted forest under 1.3 m	0.22
Recently planted forest over 1.3 m	0.15
Recently planted forest with hold-over trees	5.76
Young growing forest	9.82
Grown up growing forest	45.02
Mature forest	32.89
Shelter wood forest	0.03
Poorly productive forest	5.54
Uneven-aged forest	0

Table 3 represents the type of tree species and their mean age in the study region.

Species	Percentage	Mean age in years
Pine	38.00	38.00
Spruce	40.89	40.89
Silver birch	2.74	16.68
Downy birch	0.43	26.33
Others	17.91	0.98

3.2 Geospatial data and ground truth data

3.2.1 ground truth data

Two sets of ground data were provided namely Forest Use Notifications and Forest Stand Data. The former was used to identify stands that experienced damages while the later one was used to extract stands that were not touched by the wind (called undamaged stands). Forest Use Notifications were reports that were made by forest owners about their forest. This includes information about planning for clear cutting and thinning of their forests. In addition, owners are required to include information about possible damages that might have happened and the cause of those in this report (more can be read using links [14] and [15]). In Finland, there is a legal obligation on forest owners to make this report, which can be seen from link [16] in section 14. In the Forest Use Notification Dataset (geo-packages for each region), there is a column named "forestdamagequalifier" that meant for representing the cause of possible damages to stands. Based on documentation provided by Metsakeskus, there were different codes representing different cause of damage in the dataset, labeled 1501, 1504, 1550, 1600, and 1602. of which, code 1504 represent damages caused by winds, meaning that stands with "forestdamagequalifier" = 1504 can be regarded as stands that have some damage inside (called damaged stands). Stands that had no damages, received a null value on their "forestdamagequalifier" attribute. It is worth saying that there was no information regarding severity of damages inside each stand and also it was not clear if all the extent of stands were damaged or part of them have some damages. Forest Use Notification geo packages is available at link [4] (available in reference section). In addition, links [5] and [6] represents existing features inside these packages and some metadata about them.

The second dataset were not based on forest use notifications. They came from the forest stand data base, which is maintained by the Forest Centre in Finland and can be downloaded from this page [18]. The data aimed to cover all Finnish private forests and contains a lot of information about the forests. Link [7] represents existing feature inside this dataset. This dataset did not have any information about forest damage, therefore, damage stands could not be

identified from this dataset. It is worth saying that the border of stands in this dataset is defined by Forest Center while in the other one (Forest Use Notifications), owners themselves are responsible to define stands borders, meaning that two dataset's stands may not overlap since they come from different sources. Links [8] and [9] contain some useful information about this dataset.

The primary ground truth data sources that were used to distinguish damaged stands in this thesis were stands located in five regions close to the area that storm happened, which can be downloaded from link [4]. The damaged stands illustrated in figure 3.1 (black dots) were extracted from four regions named Uusimaa, Kymenlaakso, Kanta- Häme, Häme, and Varsinais-Suomi that are regions where the storm affected, shown in figure 3.2.

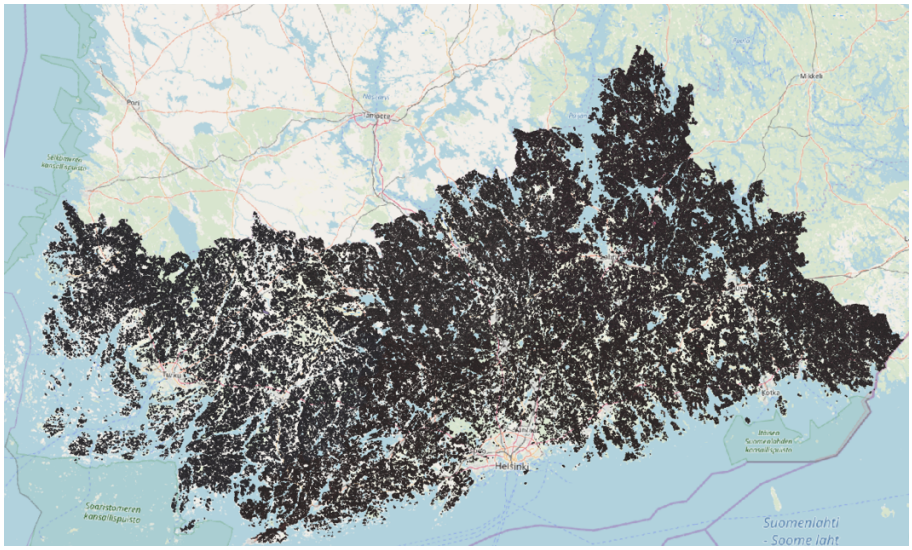

Figure 3.2- shows forest use notification in the five regions in Finland

The five mentioned downloaded geo packages were forest use notifications that were made based on owners' report. In order to only extract stands that hit by the wind invaded on 12th August 2017, named Kiira storm, two condition were taken into account:

1- The time period considered for extracting the stands was from 12th of August until 30th September. Phenology effect was the main reason for selecting this particular period of time, which was also suggested by previous studies.

2- The stands that had a value of 1504 for their attribute called "forestdamagequalifier" (wind damage qualifier code) were considered as damaged candidates.

Figure 3.3 illustrates some of the attributes available in the packages:

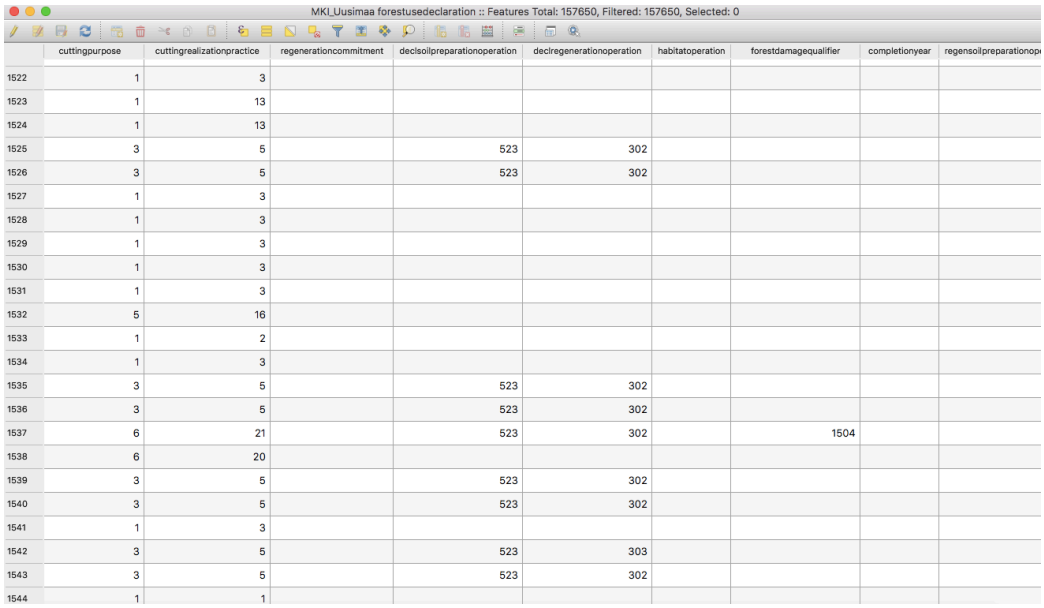

	cuttingpurpose	cuttingrealizationpractice	regenerationcommitment	declsoilpreparationoperation	declregenerationoperation	habitatoperation	forestdamagequalifier	completionyear	regensoilpreparationop
1522	1	3							
1523	1	13							
1524	1	13							
1525	3	5		523	302				
1526	3	5		523	302				
1527	1	3							
1528	1	3							
1529	1	3							
1530	1	3							
1531	1	3							
1532	5	16							
1533	1	2							
1534	1	3							
1535	3	5		523	302				
1536	3	5		523	302				
1537	6	21		523	302		1504		
1538	6	20							
1539	3	5		523	302				
1540	3	5		523	302				
1541	1	3							
1542	3	5		523	303				
1543	3	5		523	302				
1544	1	1							

Figure 3.3- illustrate some available attributes inside each forest use notification report in Uusimaa region in Finland

Considering the condition mentioned above, 692 stands in the forest use notification dataset met the requirements and extracted for the next step, which would be preprocessing of data. Figure 3.4 shows the distribution of extracted damaged stands in Helsinki region.

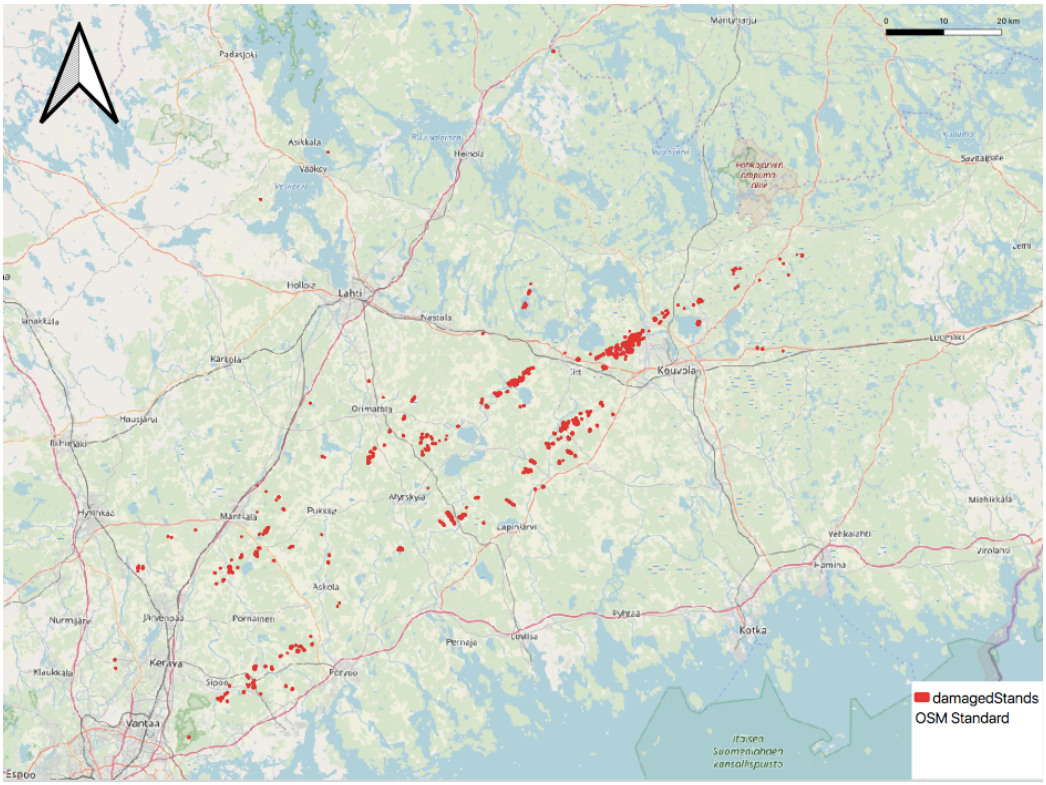

Figure 3.4 shows stands, red dots, that were hit by the wind named Kiira in Helsinki region.

As explained above, there was a second dataset that came from Forest Center in Finland, which basically was used for extracting stands with no disturbances. To differentiate stands or areas that were not touched by the storm (called undamaged stands) from ones that were hit, a spatial filter was created, to which all damaged stands geometries were introduced by taking advantage of Forest Use Notification dataset. Using this filter on the Forest Center dataset, one could easily extract undamaged stands and clip pixels that were outside areas that were assumed to be damaged. In this study, two different approaches were used to form the training data, namely average-based and pixelwise, which is explained shortly.

Figure 3.5 illustrate Forest Center data, which covered a lot of unnecessary areas that were out of the area of interest, therefore, a subset of this dataset was generated to only focus on the study areas. The right image shows the subset of dataset shown on the left image, aiming to target only the areas of interest, which was detected by the help of Forest use notification data (692 extracted stands covered) and also sensed images available in the area of interest (11th of August 2017 and 5th of September 2017):

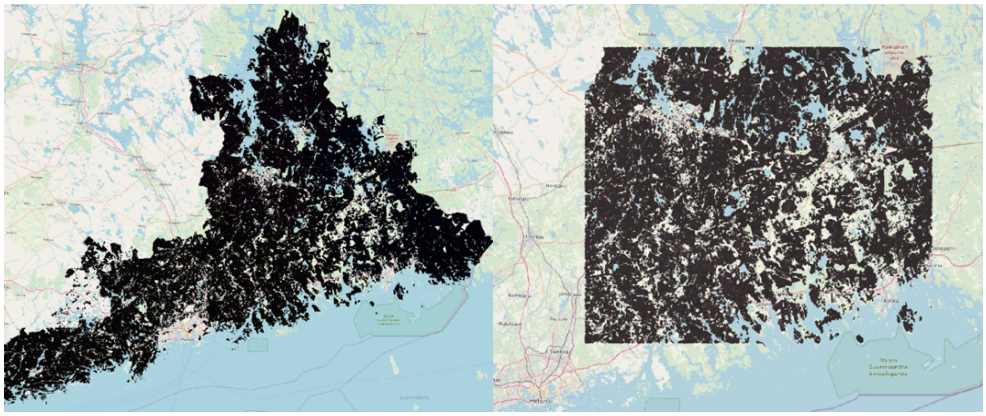

Figure 3.5 shows dataset provided by Forest Center in Finland, right image is a subset of the left image

3.2.2 Satellite data

An attempt was made to find images that are closer to the time when storm happened (12th August 2017). Of all images taken from first of June to the end of September, two images, shown in figure 3.6, had the least cloud coverage, which were taken on 11th of August and 5th of September. This step was the most time-consuming part in this thesis since in 2017, Helsinki region experienced a cloudy summer. Table 4 illustrates some metadata of the images used in this thesis:

Table 4- shows metadata about the images used in this thesis

Image id	Cloud coverage	Date taken	Sun zenith angle	Type of product	Platform
S2B_MSIL2A_20170811T095029_N0205_R079_T35VMH_20170811T095027	44%	11th August 2017	46 degree	2A	Sentinel-2B
S2A_MSIL2A_20170905T095031_N0205_R079_T35VMH_20170905T095028	25%	5th September 2017	54 degree	2A	Sentinel-2A

Both images were downloaded from ESA open hub online service that is accessible via link [10]. Figure 3.6 represents the RGB version of the images used in this thesis:

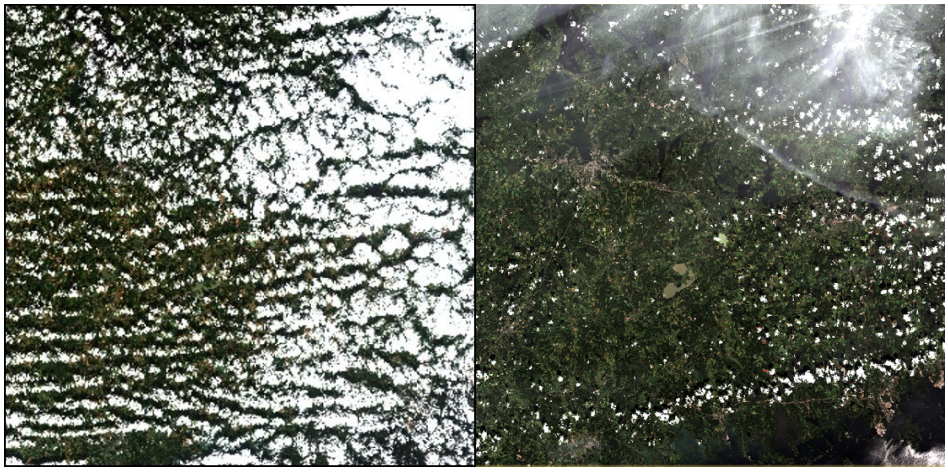

Figure 3.6 illustrate 11th of August image on the left side and 5th of September image on the right

As seen the quality of both images, especially the left one is poor. Of all images from 15th of July to the 30th of September in 2017, these two images had the least

amount of cloud coverage. The main reason why this period of time was chosen for finding the images was phenology effects that could introduce more uncertainty to the work. In addition, it was assumed that from September 2017 on, forest owners started clear cutting of their stands, which would bring inaccuracy into the work, therefore, later images were not considered in this study.

3.2.3 Non-Forest mask

A 16 by 16 meter non-forest mask, created by Natural Resource Institute Finland, (LUKE) was provided. This mask is available on the super cluster computer, named Taito, maintained by CSC via this path [11].

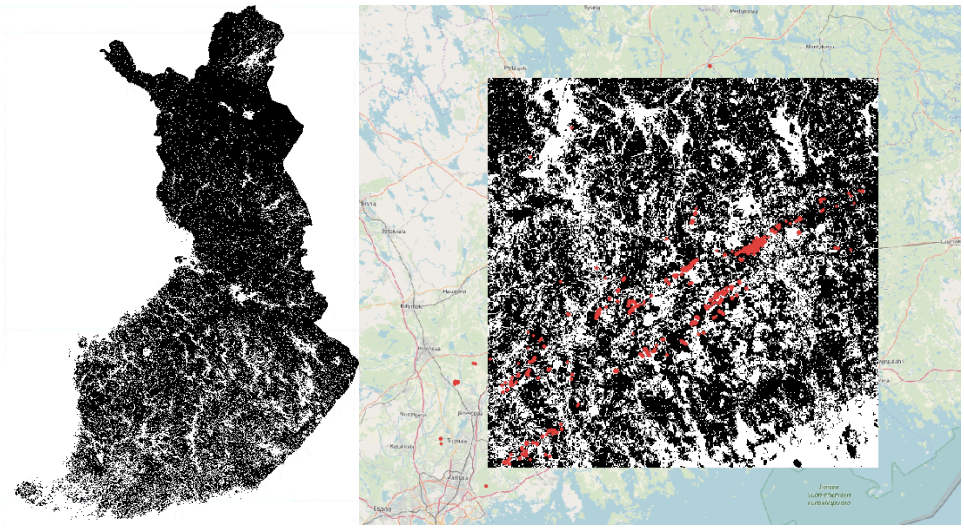

Figure 3.7 shows inventory mask for whole Finland on the left and 10-m resampled subset on the right

In order to fit 16-meter resolution with 10-meter bands used for analysis, GDAL library was used. Documentation about this mask can be downloaded using link [12]. This documentation reports methods and results achieved from the Finnish multi-source forest inventory in 2015. It meant for helping users to understand how products were made and have an idea of benefit and limitations they can get from the products. In order to generate these products, several geospatial sources were used namely satellite data, field data, digital maps. More can be read via links [12] and [13].

3.2.4 Selected bands

In this thesis, an attempt was made to select indices that were taking advantage of near infrared and red bands because such indices were able to expose the spectra behavior of vegetation due to presence of Chlorophyll inside leaves. Considering literature review and previous work done on detection of wind damages, it was exposed that NDMI, NDREI, NDVI, SATVI, EVI, TCB, and TCG could be considered for detection of disturbances occurred in forest areas. As mentioned in literature review, Stych et al., (2019) concluded that using indices that take advantage of SWIR, NIR, and RED could be highly effective in detection of storm damages. Einzmann et al., (2017) also concluded that indices that enjoyed the use of red edge and blue bands such as PSRI, NDREDI played the most important role in detection of disturbances using random forest classifier. Wang et al (2009) also used and compared the effect of different indices using different change detection algorithm in detection of storm damage in forest and concluded that indices that benefit from SWIR1 and SWIR2 could perform well. They also suggested indices that uses RED and NIR could be beneficial for storm damage detection.

The reason for using all these 6 indices as predictors altogether in this study was that the selected indices target and measure different features, which could bring their own variance to the models. Even if they meant for measuring the same thing, they usually perform differently in different conditions. For instance, NDVI and EVI target green mass, however, when leaf area index (LAI) is higher than a certain amount (1.8), NDVI saturates, which causes inaccuracy in damage extraction. This issue would be critical especially when the rate of damage is small. It would have been possible to keep only one of these indices (NDVI or EVI) if there was information about LAI of study area.

3.2.5 Image pre-processing

Initially, resampling was applied to the bands 5, 11, and 12 to make them consistent with the bands 2, 3, and 4 that were in 10-meter resolution. To implement this, GDAL library on Python 3 was used. Sentinel scene classification (SCL) band also needed resampling from 20 meter to 10 meter, which was done in this step.

1- Noise removal:

Two different filters were applied on each band. The first one came from the images themselves, which was scene classification band (SCL). This mask was used to remove pixels that were not in our interest, namely snow, water, cirrus, shadows. The whole table and its assigned label can be seen in figure 3.8. More about this mask and how it is generated can be read via link [17].

Label	Classification
0	NO_DATA
1	SATURATED_OR_DEFECTIVE
2	DARK_AREA_PIXELS
3	CLOUD_SHADOWS
4	VEGETATION
5	NOT_VEGETATED
6	WATER
7	UNCLASSIFIED
8	CLOUD_MEDIUM_PROBABILITY
9	CLOUD_HIGH_PROBABILITY
10	THIN_CIRRUS
11	SNOW

Figure 3.8 shows scene classification table of Sentinel-2 products [17]

Considering the scene classification table shown in figure 3.8, the algorithm kept all pixels that had value of 4, assigned to vegetation, untouched while zeroed the others. To implement this in practice, all chosen bands for this study and the SCL mask were stacked using Numpy library on Python 3. Then, considering the value of pixels in SCL band, the algorithm zeroed all pixels that their corresponding SCL were other than value of 4 and kept the values of the rest untouched.

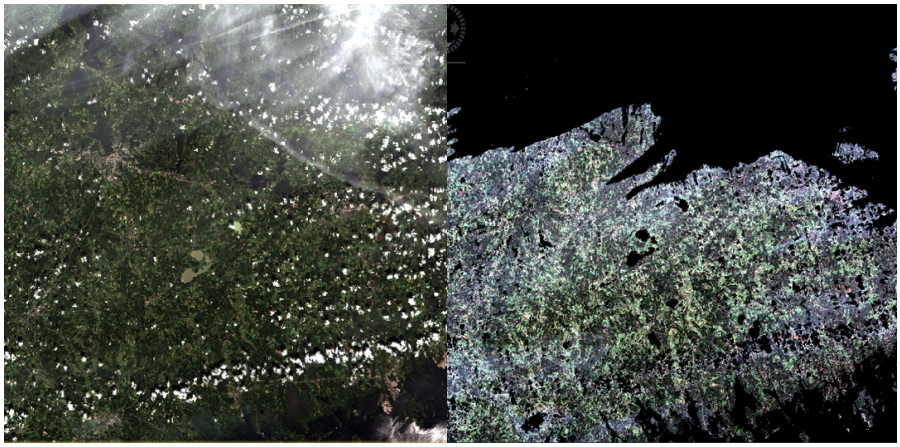

Figure 3.9 shows the image taken on 11th of August 2017, the left one is the original RGB and the right one is the masked version

Figure 3.9 represents image taken on 11th of August 2017 before and after applying the first mask (SCL mask).

The dark pixels on the right image received zero values, which were mostly clouds and water. Similarly, the same procedure was applied on the post scene in which there was more effects of clouds, therefore, it was expected that considerable number of pixels would be assigned to zero.

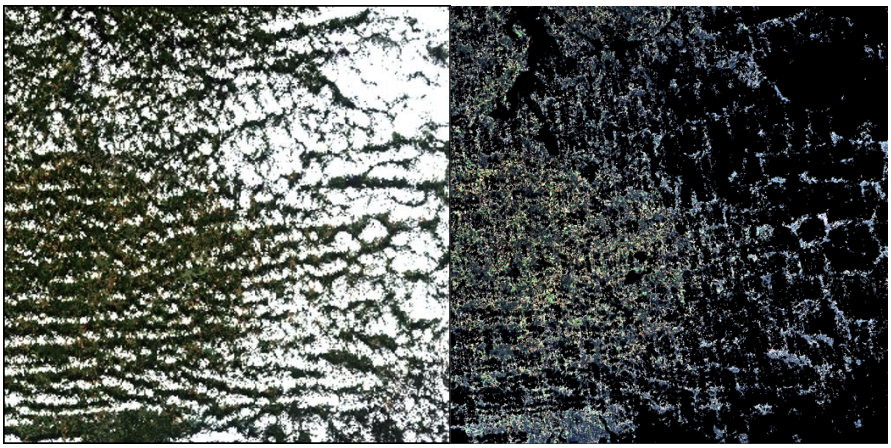

Figure 3.10 shows the image taken on 5th of September 2017, the left one is the original RGB and the right one is the masked version

Figure 3.10 illustrates the post scene taken on 5th of September 2017.

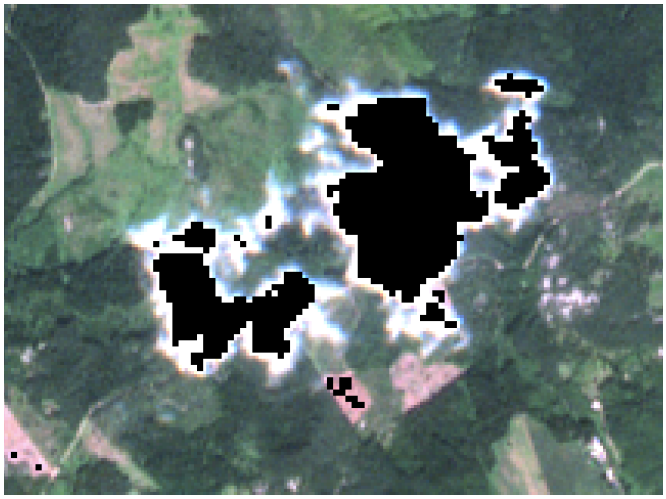

Figure 3.11 shows the cloud noise left after the SCL mask applied

Figure 3.11 illustrate that SCL mask was not efficient enough to remove all the cloud noises:

To address this issue and remove it from upcoming calculations, it was necessary to find the signature of the remaining cloudy pixels. Image segmentation was applied using an K-means algorithm. The C parameter, number of centroids or classes, and i , number of iterations, were set to 5 and 90 respectively. It revealed 4 signatures existing in the scene using band 2, 3, 4, 5 and 8 which can be seen from figure 3.12. The main reason for selecting these bands was that they could expose vegetation spectra changes the best. Visible light is absorbed by healthy vegetation while near infrared is reflected, therefore, by using the selected bands one may be able to exclude vegetation and try to find cloud signature.

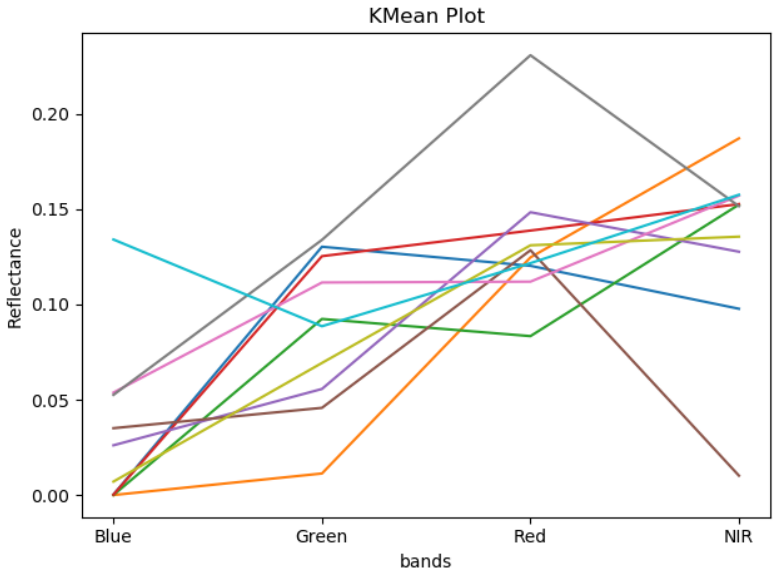

Figure 3.12 represents k-means results on the pre-image

Looking at figure 3.12, inferring the signatures that belonged to clouds was difficult since each signature could present any existing land cover in the scenes. This step usually needs expertise and some extra exploration. Of course, one way to manage this is applying every signature one at a time and then evaluating and comparing the results to discover which one is more effective in the removal of noises, which would be really time consuming especially if the number of features (classes) is more than 10. To minimize this effort in this study, an attempt was done to determine the approximate range of the noisy pixels in the images by manually hovering the cursor on the cloudy pixels and clicking on the noisy pixels using a 4-band image that contains bands, namely blue, green, red, and near infrared on QGIS Desktop Application. By this, it was exposed that remaining cloudy pixels had reflectance values of more than 0.1 on the almost all bands used. Considering figure 3.12, there were two signatures that met this condition. After applying each at a time and comparing results visually, it turned out that the dark line (the first signature from up) was the one that could effectively eliminate most of the remaining cloud noise from the image and keep the healthy ones untouched. an estimate of the rang of noisy pixels was achieved.

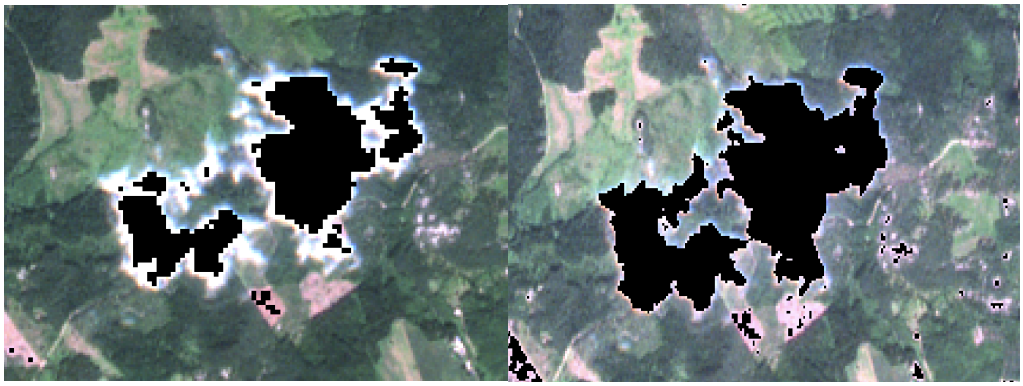

Figure 3.13- right image is the rectified version of the left one after second filter was applied

Figure 3.13 shows the effect of the second filter on the remaining noise from the SCL mask.

This step was done for both scenes (pre-storm and post-storm), meaning that for each one, different cloud signature was detected. By using those signatures on the corresponding bands, considerable number of remaining cloudy pixels were assigned to zero, meaning they were ignored from the upcoming calculations. It is worth to say that there were no worries about removing important pixels (such as forests) since they had reflectance values of less than 0.1 on the used bands. This was discovered by the same strategy used to find the range of cloudy pixels.

2- Applying inventory mask:

This mask was applied after removal of cloudy pixels and meant for targeting only forest areas, meaning that all pixels that did not belong to any forest type were assigned to zero values.

3.2.6 Changed feature extraction

Univariate image differencing (UID) was used as change extraction algorithm for this study. UID was simply calculated by subtracting post-image from pre-image, by which any changes in the spectral response could be monitored. The reason for choosing this extraction algorithm was its simplicity and popularity in the previous studies. Assuming no other factors interfered beside the disturbances caused by Kiira storm, UID created a continual change imagery in which pixels with negative values represented damaged forests and pixels with either zero or posive values went for undamaged forests. Grybas et al., (2015), Vorovencii et al., (2014), and Wang et al., (2009) also used UID as change extraction method in their works and the final results were satisfying.

Table 5 shows all the methods used in this study. Each individual method was used an independent predictive variable in the models. To implement these methods and calculate the image differencing, the following packages used on Python 3, namely GDAL, SCIPY, and NUMPY.

Table 5-methods

Method	Abbreviation	Formula
Image Differencing of NDVI bands	NDVI	$(NDVI_b - NDVI_a)$
Image Differencing of tasseled cap brightness bands	TCB	$(TCB_b - TCB_a)$
Image Differencing of tasseled cap greenness bands	TCG	$(TCG_b - TCG_a)$
Image Differencing of NDMI bands	NDMI	$(NDMI_b - NDMI_a)$
Image Differencing of normalized difference red edge bands	NDREI	$(NDREI_b - NDREI_a)$
Image Differencing of enhanced vegetation index bands	EVI	$(EVI_b - EVI_a)$
Image Differencing of soil adjusted total vegetation index bands	SATVI	$(SATVI_b - SATVI_a)$

3.2.7 Pixelwise approach

The goal of this approach was to have a binary raster map in which users can easily identify the location of wind disturbances in forest. To manage this, individual pixels were used to train the classifiers. In order to extract pixels assumed as damaged, forest use notification data were used. All the stands that met the two requirements (the time and the damage qualifier explained before) were selected, 692 stands, which had an overall area of 1498 ha. In order to clip pixels inside these stands, their geometries were used as a spatial filter on the images, ending up with 42375 pixels labeled as damaged. It is worth saying that the ratio of pixels labeled as damaged to pixels that could be candidates for undamaged class in the whole extent of image was 0.0004, meaning that the frequency ratio of the two classes in the whole image was 0.0004. For the other class, undamaged, Forest Center dataset was used. To avoid clipping pixels that already were assumed to be damaged, the algorithm randomly clipped 45000 pixels whose geometry were not inside or in touch with damaged stands borders.

After calculation of all methods using GDAL and NUMPY on Python 3, there were 7 image-difference products in hand, namely NDVI image difference, NDMI image difference, SATVI image difference, TCG image difference, EVI image difference, NDREI image difference, and TCB image difference, which were ready to be used as independent predictors inside the models. As explained above, to clip pixels and assigned them to their appropriate classes, Forest Use Notification's stands geometries were used. After clipping, there were 42375 and 45000 pixel values for each individual predictor, which was labeled as damaged and undamaged respectively. This formed a balanced pixelwise dataset from which the training, evaluation and test datasets were formed.

Before starting training, 30 percent of the pixelwise dataset was separated in order to be unseen, which was named pixelwise test dataset. The rest, 70 percent, was used for training and evaluation of the classifiers. Both datasets were almost balanced since they were created from a balanced dataset. As explained above, it was critical to have balanced data for training to avoid biased decision in which minority class, either classes, would be underestimated. However, this is not the case for testing, meaning that a well-trained model should be able to perform well on both balanced and unbalanced test data. Considering the poor quality of

imagery used and the fact that probably almost all images that would be used later for prediction would have a totally unbalanced dataset such as ones used in this study (ratio of 0.0004 between classes), an unbalanced test data in which the ratio between the classes was 0.0004 was manually generated using the existing balanced dataset. As a result, there were two test data sets in the testing step. One had almost a balanced combination of the two classes and the other one that was manually formed (dropping enough damaged pixels to reach ratio of 0.0004) from the first balanced test data to meet the required ratio.
Table 6 illustrate the random forest configuration setup used:

Table 6-represents configuration used to build random forest classifier

Number of trees in the forest	Criterion	Min sample split	Max feature
900	Gini	2	Auto

To implement the shallow model, RF, Scikit-learn package on Python 3 was used.

In order to establish the deep model, NN, Tensorflow and Keras packages on Python 3 were used. Table 7 illustrates the initial setup used for creation of the fully connected network, NN. It is worth saying that the initial setup had random parameters such as number of deep layers, neurons, epochs, and activation function.

Table 7-illustrates configuration of fully connected layer (initial setup)

Number of dense layers	Activation function	Loss function	Optimizer	Regularization technique	Neurons	Epochs
8	RELU	Binary cross-entropy	Adam	None	64	50

To find the best parameters, there was a need for another set of data called validation dataset. To achieve this, for each epoch 75 percent of training dataset was used for training the model and the remaining 25 percent was used to validate the model. Figure 3.14 represents the performance of NN using initial configuration setup on training and validation datasets. It was obvious from the figure 3.14 that it was about epoch 25 when the model started overfitting and the validation loss stopped improving and started getting worse. To address this issue, one of the most common regularization technique, known as dropout, was applied. Figure 3.15 shows the effect of dropout technique on the performance of the model. As seen, both validation and training accuracy improves while loss score was diminishing for both. In order to estimate the other parameters such as number of neurons, layers and activation function, trial and exam strategy was used, meaning that by applying different range of parameters and having an eye on the training and validation plot generated in each epoch, the final parameters of the NN were estimated. Table 8 shows the final configuration setup on NN used in pixelwise approach.

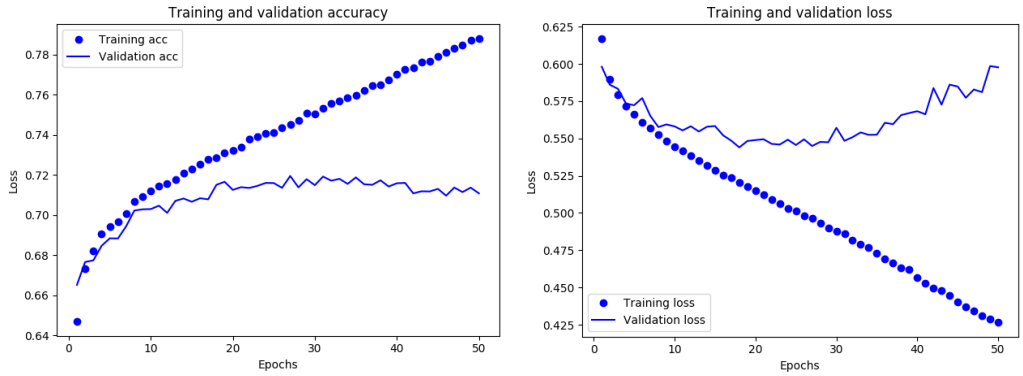

Figure 3.14 illustrates validation accuracy and loss score achieved by the initial configuration setup of the model

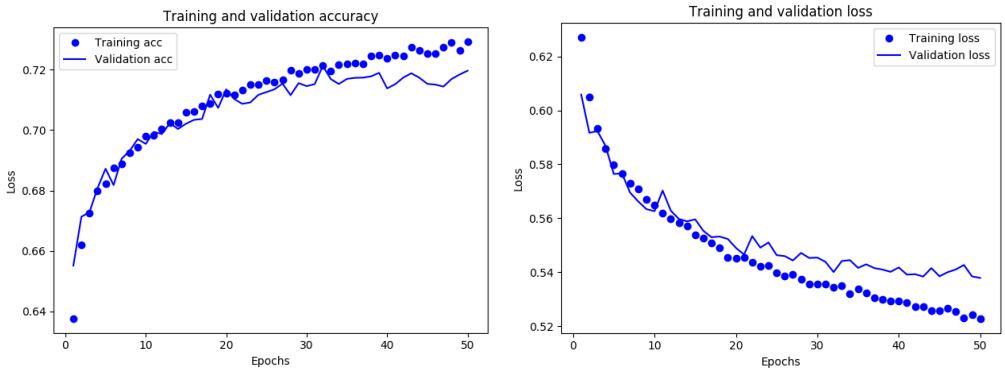

Figure 3.15 shows validation accuracy and loss score achieved after regularization technique was applied on NN

Table 8-shows the final configuration setup of NN in pixelwise approach

Number of dense layers	Activation function	Loss function	Optimizer	Regularization technique	Neurons	Epochs
10	RELU	Binary cross-entropy	Adam	Dropout=0.2	128	50

Once the final configuration setup of the models was determined, K-fold cross validation technique was applied using the training dataset followed by final training (trained by all 70 percent of training data at once) and testing the models by taking advantage of test data that was never seen by the models.

3.2.8 Average-based approach

Since individual pixels could be noisy, especially in this case of study where images were not enjoying a good quality, it was decided to calculate the mean of each stand, meaning that each stand would represent one observation. By doing this, it was expected to achieve more reliable results. Two different strategies taken to form two datasets for this approach. In the first strategy, for the undamaged class, 700 stands were randomly chosen from the whole extent of the image while for the second one, 700 stands were randomly selected from a subset of the image. It is worth saying that the other class, named damaged, was the same for both, which was 692 stands that was generated based on forest use notifications. As a result, in this approach there were two datasets, which offered their own training, validation, and test datasets. The reason for creation of two different sets of data was that each sentinel image covered a 100 km by 100 km area on the ground, therefore, for each image it was assumed that the effect of atmosphere was the same on all extent of area covered, which in reality may not have been true. Consequently, this fact contributed to creation of the second dataset, generated by the subset of the image in which only the neighborhood of areas reported as damaged were considered.

The first dataset was easily generated by adding 700 randomly selected stands, assumed as damaged, extracted from the entire extent of the image to the forest use notification dataset, containing 692 stands known as damaged. Exploring into the dataset, it was exposed that some stands contained too few pixels, meaning that there was a high possibility that the vital pixels might have been eliminated and the few left might not have represented what a particular stand labeled for, which would bring inaccuracy into the work. In order to address this issue, a customized filter was created to check the pixel coverage of each individual stand in the dataset, meaning that if any stand had less than 80 percent pixel coverage, that stand was eliminated. In practice, this was done by calculating and comparing the area of each stand and sum their corresponding pixels inside. Of all 692 stands labeled as damaged, 132 met the requirement and for the other class, damaged, 228 stands passed the set criteria, meaning that the first dataset used in average-based contained 360 data points overall for the

further processing. Figure 3.16 shows the distribution of data points in the first dataset.

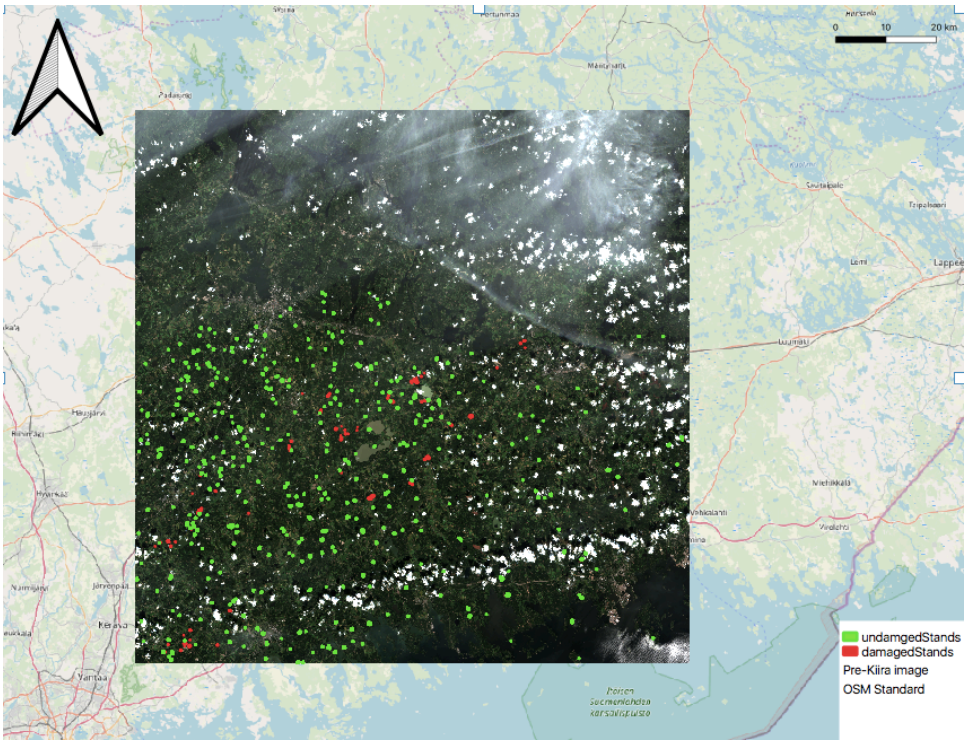

Figure 3.16 shows distribution of the two classes in the first dataset used in average-based approach

As explained briefly above, the second dataset was created based on a subset of the image. For this dataset, the previous 132 damaged stands that had at least 80 percent pixel coverage remained the same, however, the only difference was that new 228 undamaged stands that were randomly selected from the subset of image where undamaged stands would be much closer to the damaged stands. It is worth saying that the same criteria of having at least 80 percent pixel coverage was considered as looking for new undamaged stands. By this, the focus was highly on only regions hit by the storm. To create this the subset of the image, first a 3 km-buffer was made around each damaged stand, which can be seen in figure 3.17.

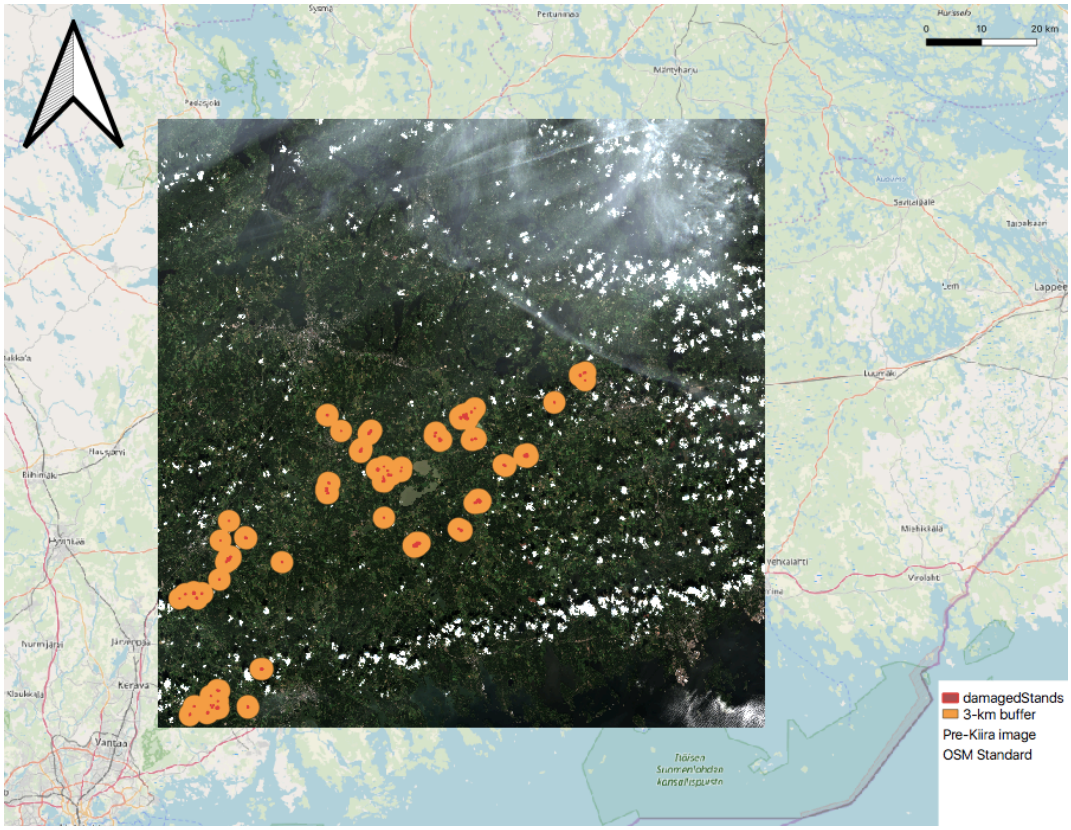

Figure 3.17 illustrates 3-km buffer around damaged stands

In the next step, a manual buffer was made in such a way that surrounded all the buffered stands using QGIS Desktop Application. Figure 3.18 represents the manual buffer that contained the area in which new undamaged stands would be selected. By doing this, the area of study region diminished to 281404 ha, meaning that the second dataset in average based was coming from a much smaller region shown in figure 3.19.

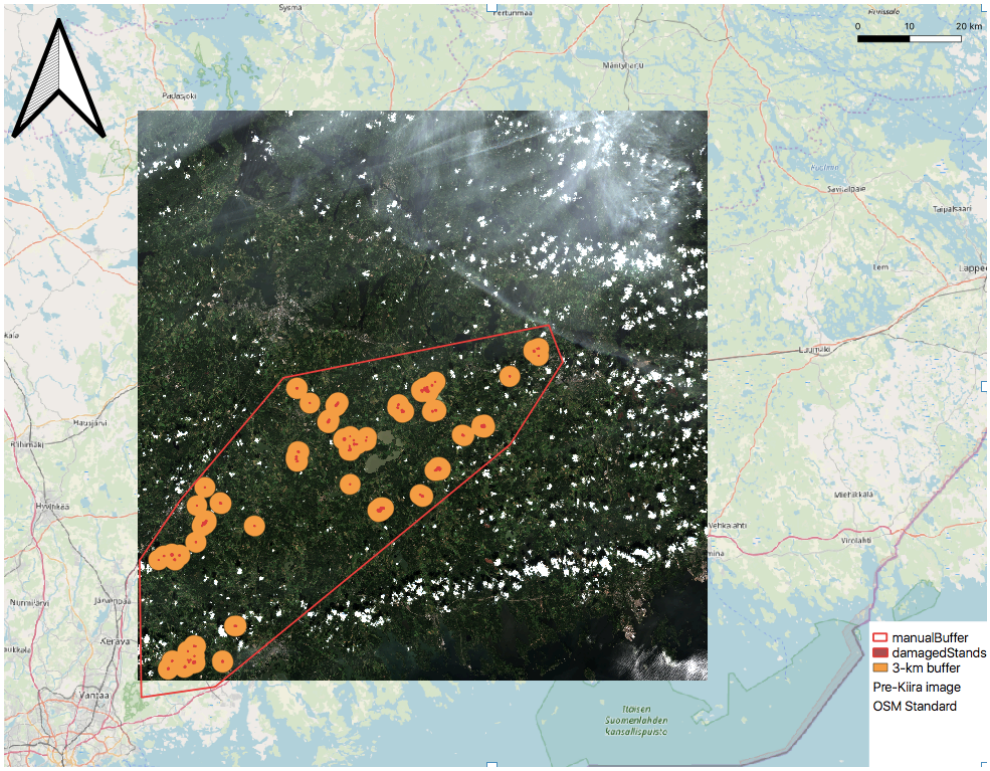

Figure 3.18 shows manual buffer created around damaged stands

Considering the manual buffer, 228 stands, labeled as undamaged, were randomly selected in the surrounded area. Figure 3.19 illustrates distribution of data points in the second data set.

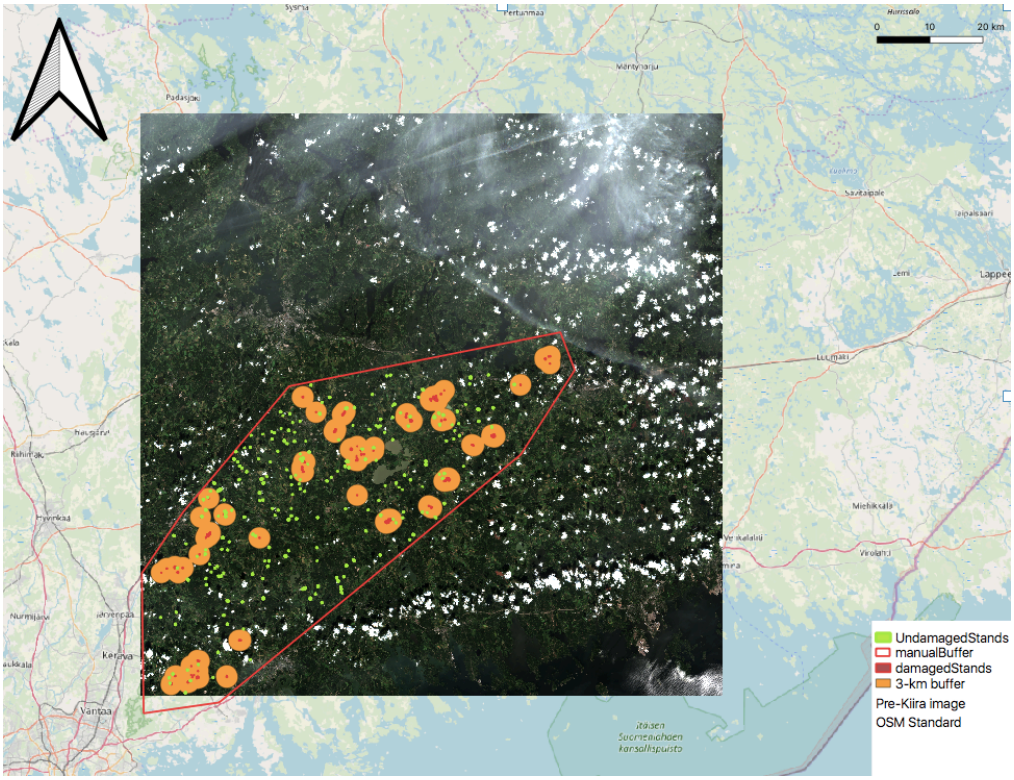

Figure 3.19 illustrates distribution of all data points used in the second dataset

Once the two datasets were generated and ready for further processing, the same workflow explained in pixelwise section was taken for creating training and test datasets, meaning that 70 percent of data in each dataset was separated for training and validation and the remaining 30-percent was untouched for the final testing of the classifiers.

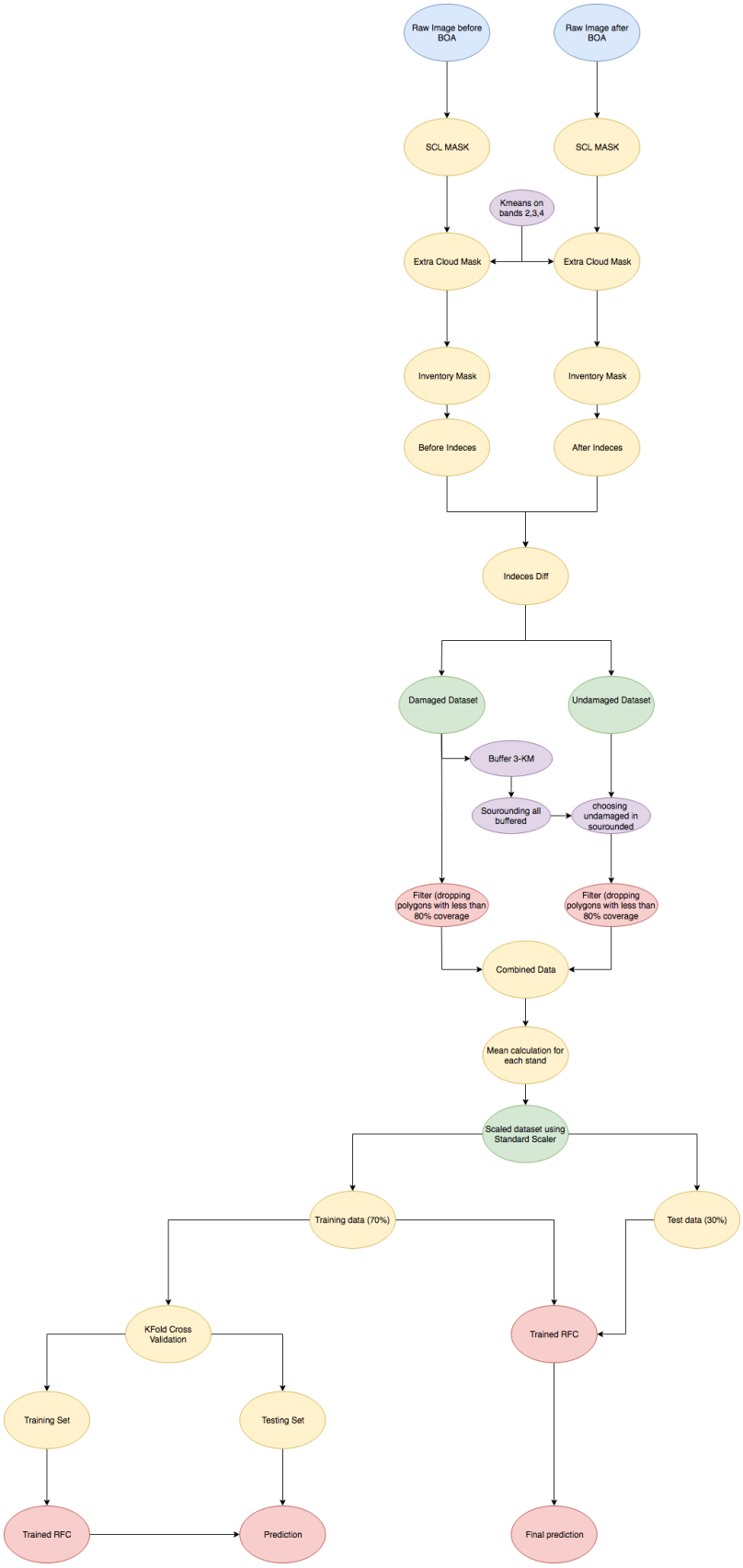

Figure 3.20 shows the workflow followed during implementation of average based approach on RF

4. Results

Considering the methods used in this thesis, namely NDVI, TCB, NDMI, TCG, SATVI, EVI, and NDREI image differencing, no considerable gap was observed between the two classes, damaged and undamaged, which can be seen from figure 4.1. Blue color represents undamaged pixels while red one goes for damaged pixels. Visually inspecting, it seemed that NDMI and TCB image difference values for the two classes were slightly separated, however, NDVI, EVI, and NDREI image differences seemed to have the most difficulties to find any separation between the two classes, meaning that the value of pixels for both classes were behaving almost the same, which is also obvious from the figure 4.1.

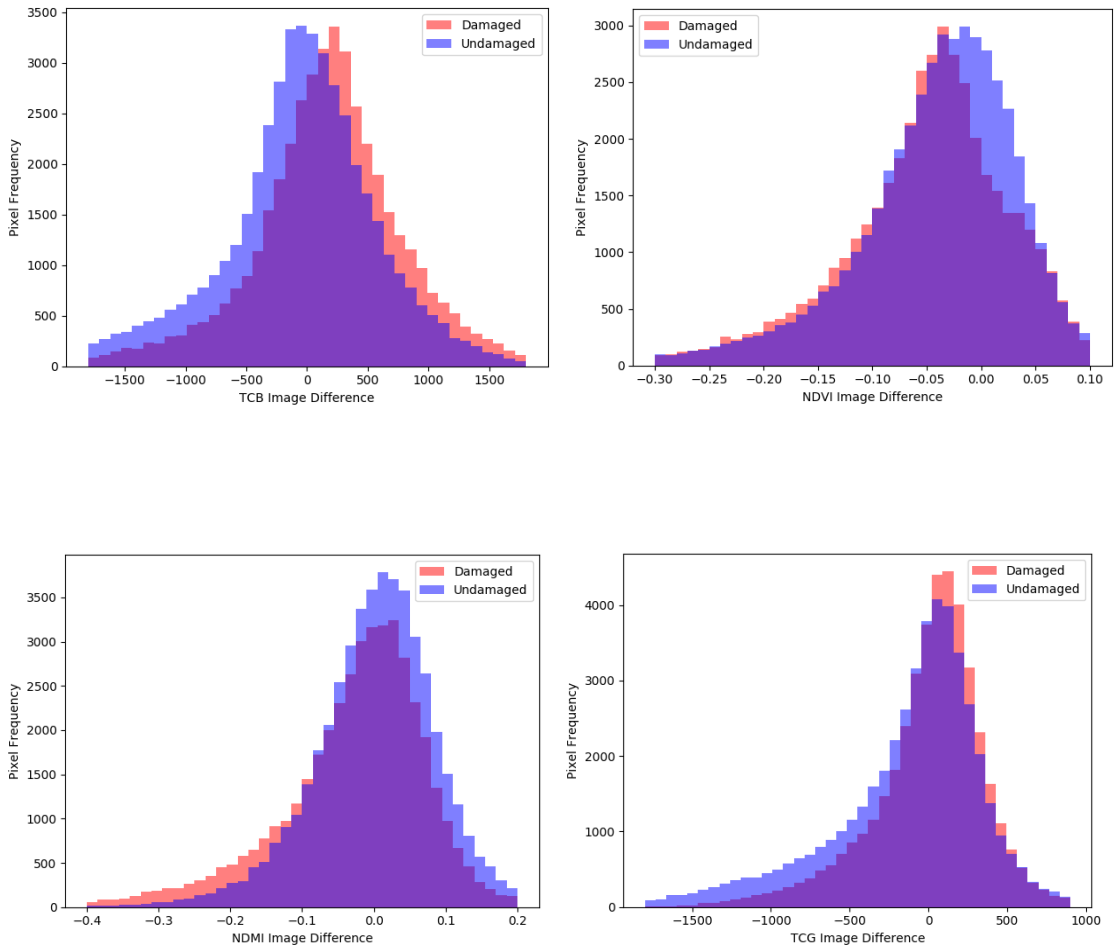

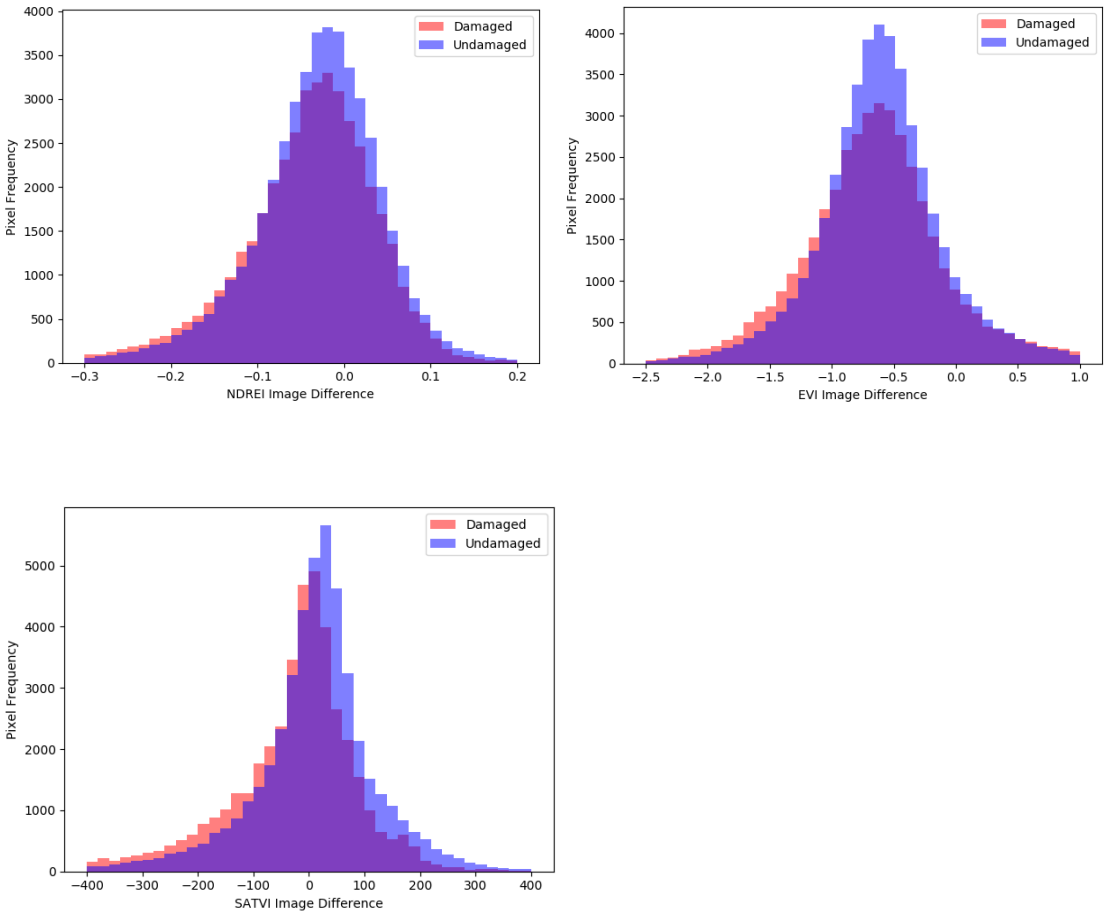

Figure 4.1 shows there was no strong gap between the two histogram of classes using different methods.

4.1 Pixelwise results

Considering K=4, table 4.1 represents an average result of k-fold cross validation achieved during four folds by random forest classifier. As seen from the table, user accuracy and producer accuracy average in four folds were almost the same as 70 percent.

Table 4.1-shows K-fold cross validation results achieved by random forest classifier

	User accuracy	Producer accuracy	F1-score	Support
Undamaged	0.71	0.75	0.73	11741
Damaged	0.71	0.66	0.68	10755
Avg/total	0.71	0.71	0.71	22496

Table 4.2 illustrates K-fold validation average results achieved by the fully connected network. It is clear that NN's user and producer accuracy remained about 70 percent.

Table 4.2 illustrates k-fold cross validation results achieved by NN

	User accuracy	Producer accuracy	F1-score	Support
Undamaged	0.73	0.74	0.73	11741
Damaged	0.71	0.70	0.70	10755
Avg/total	0.72	0.72	0.72	22496

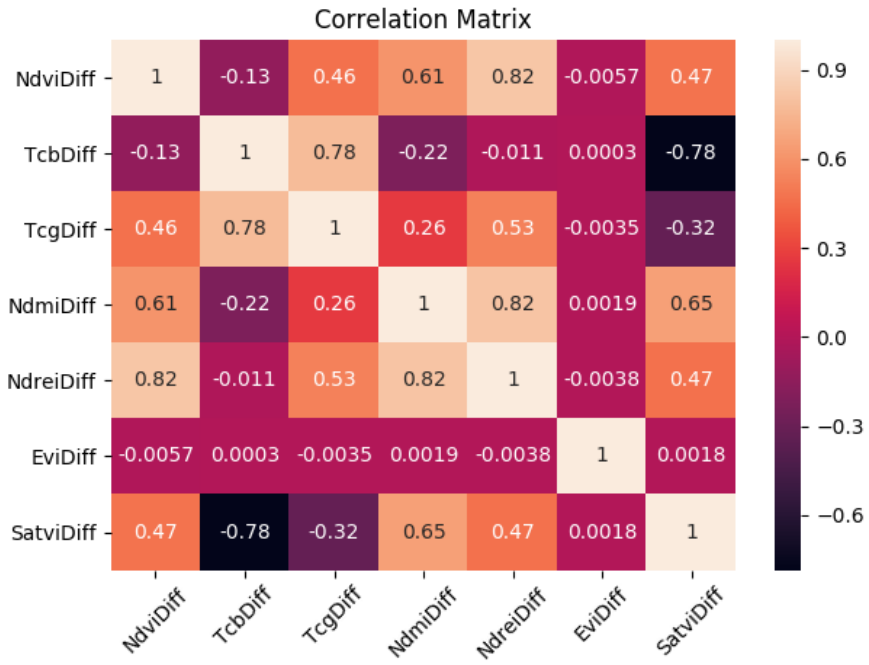

Figure 4.2 shows correlation between different methods used as predictors in the classifiers

Figure 4.2 represents correlation matrix achieved by the classifiers. It is clear that the highest correlation happened between NDREI and NDMI as well as TCG and TCB image difference methods, which was about 80 percent.

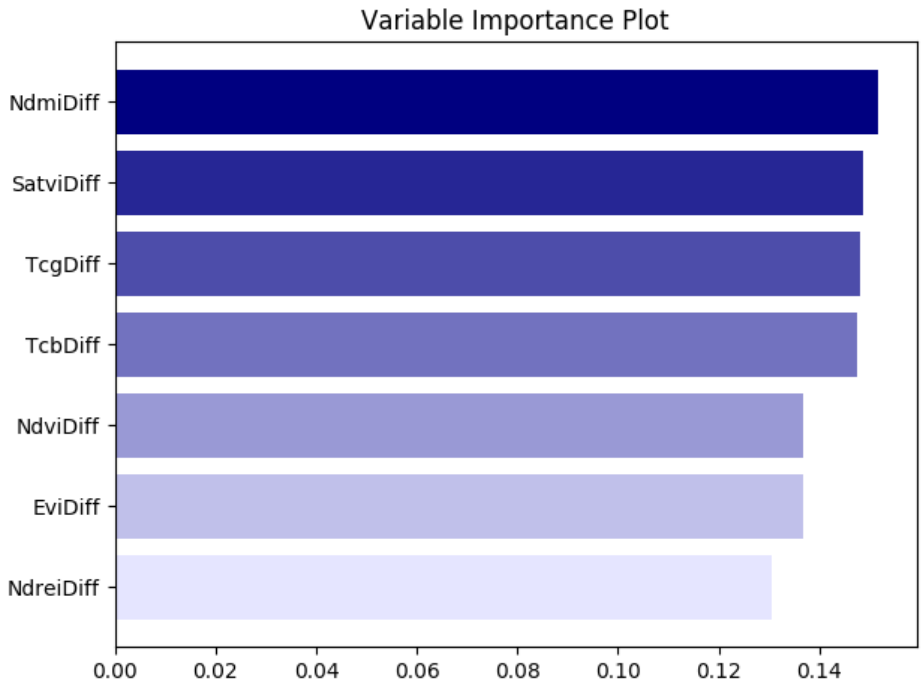

Figure 4.3 illustrates variable importance plot achieved in pixelwise approach

Of all predictive variables (methods) used on the classifiers, NDMI and SATVI were the most effective ones, meaning that they brought more variance into the classifiers compared to the others. On the other hand, NDREI and EVI performed the worst, which can be seen from the figure 4.3.

The user and producer accuracy achieved by RF on balanced test data was about 70 percent, which is obvious from table 4.3. However, using the unbalanced test dataset, the accuracy diminished sharply. In other words, RF failed to separate the classes appropriately, which is shown in table 4.4.

Table 4.3 illustrates classification report for RF on balanced dataset

	User accuracy	Producer accuracy	F1-score	Support
Undamaged	0.71	0.74	0.73	14200
Damaged	0.70	0.67	0.68	12796
Avg/total	0.71	0.71	0.71	226996

Table 4.4 illustrates classification report for RF on the unbalanced dataset

	User accuracy	Producer accuracy	F1-score	Support
Undamaged	1.00	0.75	0.86	10000
Damaged	0.00	0.75	0.00	4
Avg/total	1.00	0.75	0.86	10004

Similarly, NN performed almost as good as RF on the balanced test data, which was approximately 70 percent for user and producer accuracy, which is obvious from classification report shown in table 4.5. However, on the unbalanced dataset, it also failed to differentiate between the two classes, which can be seen from figure 4.6.

Table 4.5 represents classification report for NN on the balanced dataset

	User accuracy	Producer accuracy	F1-score	Support
Undamaged	0.73	0.76	0.74	14198
Damaged	0.72	0.69	0.71	12798
Avg/total	0.73	0.73	0.73	26996

Table 4.6 shows classification report for NN on the unbalanced dataset

	User accuracy	Producer accuracy	F1-score	Support
Undamaged	1.00	0.75	0.86	10000
Damaged	0.00	1.00	0.00	4
Avg/total	1.00	0.75	0.86	10004

4.2 Average-based results

Considering the methods used in the average-based approach, it seemed that SATVI, NDMI, and NDVI image differences managed to separate the classes better than the others, which can be seen in figure 4.4. In this approach, the vertical access shows the frequency of stands in each class while in the former approach, pixelwise, it represented frequency of individual pixels.

As explained before, in average-based approach there were two different datasets, of which the first one was formed from the whole extent of image while the second used the subset of the image.

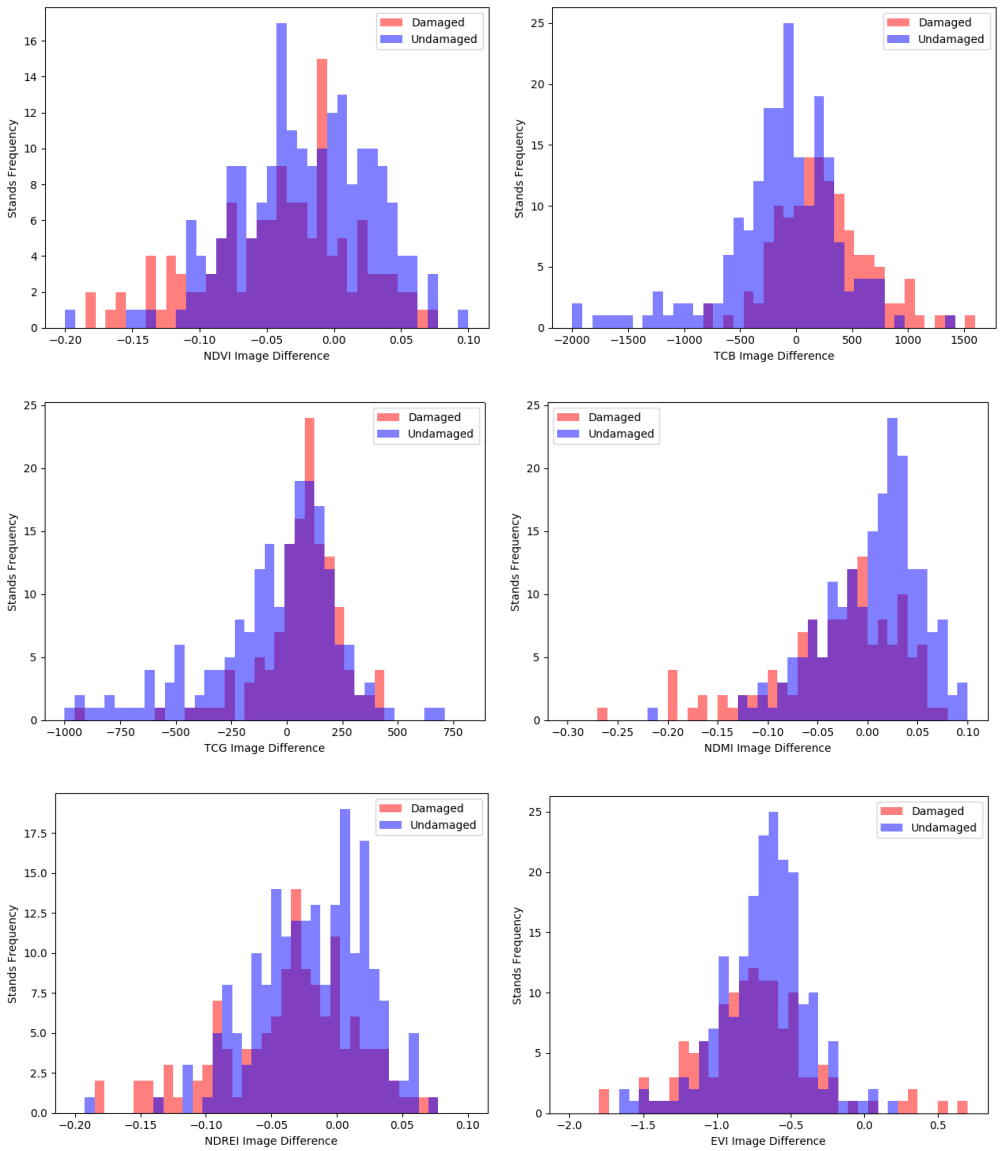

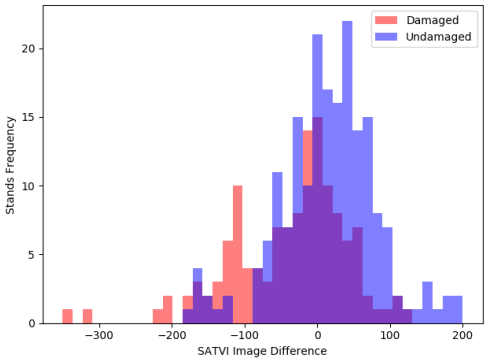

Figure 4.4 shows histogram of the methods used in this study

4.2.1 First dataset results

Considering cross validation results, both classifiers saw 10 percent improvement in their user and producer accuracies, which is clear from table 4.7 and 4.8.

Table 4.7 shows k-fold cross validation average results on random forest classifier

	User accuracy	Producer accuracy	F1-score	Support
Undamaged	0.82	0.89	0.86	73
Damaged	0.74	0.62	0.68	47
Avg/total	0.79	0.80	0.80	120

Table 4.8 illustrates k-fold cross validation average results on fully connected classifier (NN)

	User accuracy	Producer accuracy	F1-score	Support
Undamaged	0.82	0.89	0.86	73
Damaged	0.74	0.62	0.68	47
Avg/total	0.79	0.78	0.80	120

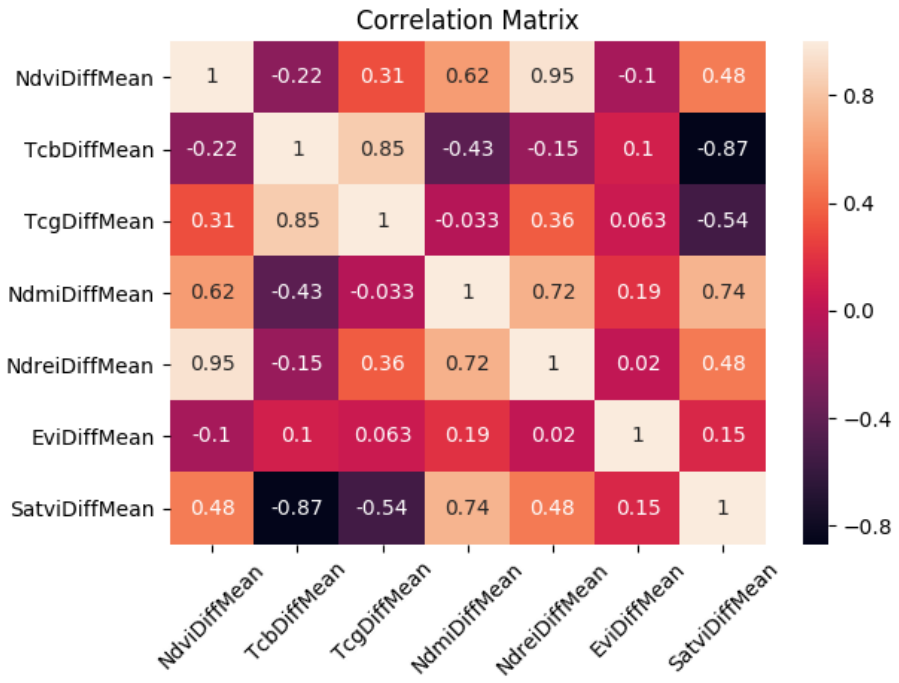

Figure 4.5 illustrates correlation between different methods used as predictors in the classifiers

High positive correlation was reported between NDREI and two other methods namely NDMI and NDVI, which was about 0.72 and 0.95 percent respectively. In addition, there was a positive 62 percent correlation between NDVI and NDMI, which can be seen from figure 4.5.

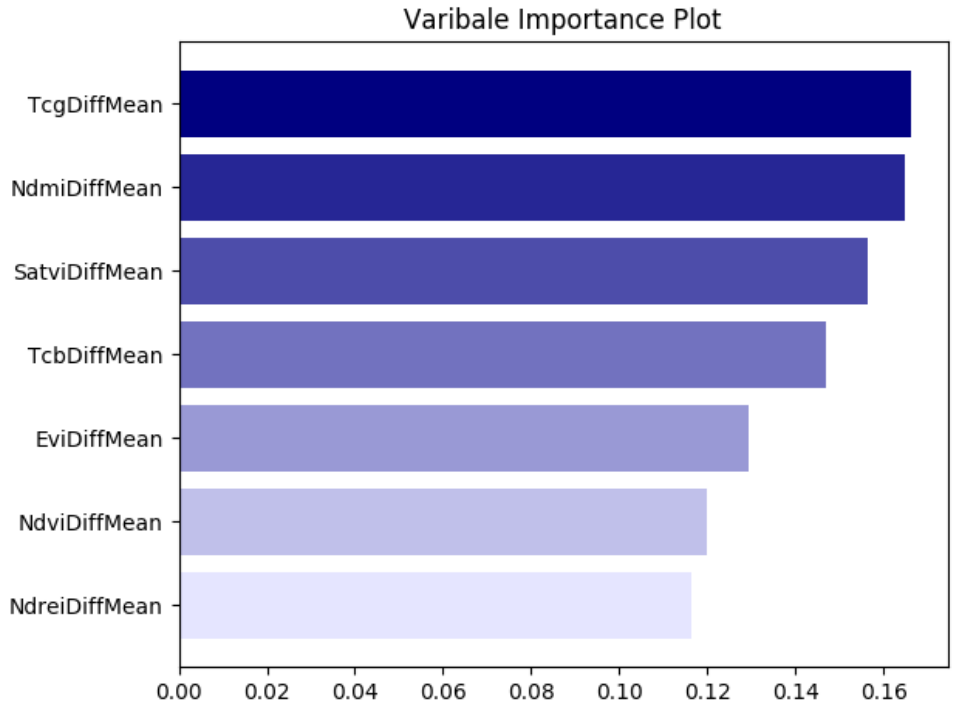

Figure 4.6 shows variable importance plot achieved in average-based using the first dataset

The most efficient methods in average-based using first dataset were TCG and NDMI image difference while SATVI stood at the third place. However, NDREI and NDVI imported the least variance into the models, which is clear from figure 4.6.

Applying the test dataset on the models, both RF and NN experienced a 10-percent improvement in their user and producer accuracy in average using balanced test dataset extracted from the test dataset, which is obvious from table 4.9 and 4.11, however, they both failed to classify damaged stands from undamaged ones when unbalanced test dataset was tried, which is seen in table 4.10 and 4.12.

Table 4.9 represents classification report for RF on the balanced test dataset

	User accuracy	Producer accuracy	F1-score	Support
Undamaged	0.81	0.86	0.85	56
Damaged	0.76	0.74	0.75	34
Avg/total	0.81	0.81	0.81	90

Table 4.10 shows classification report for RF on the unbalanced test dataset

	User accuracy	Producer accuracy	F1-score	Support
Undamaged	1.00	0.85	0.92	10000
Damaged	0.00	0.75	0.00	4
Avg/total	1.00	0.85	0.92	10004

Table 4.11 illustrates classification report for NN on the balanced test dataset

	User accuracy	Producer accuracy	F1-score	Support
Undamaged	0.86	0.90	0.88	61
Damaged	0.77	0.69	0.73	29
Avg/total	0.83	0.83	0.83	90

Table 4.12 represents classification report for NN on the unbalanced test dataset

	User accuracy	Producer accuracy	F1-score	Support
Undamaged	1.00	0.84	0.91	10000
Damaged	0.00	0.75	0.00	4
Avg/total	1.00	0.84	0.91	10004

4.2.2 Second dataset results

Considering cross validation results for this dataset, both classifiers performed almost the same. RF managed a user accuracy of 81 percent while NN reached 82 percent in average. These can be seen from table 4.13 and 4.14.

Table 4.13 represents k-fold cross validation average results on random forest classifier

	User accuracy	Producer accuracy	F1-score	Support
Undamaged	0.82	0.89	0.85	82
Damaged	0.80	0.68	0.74	38
Avg/total	0.81	0.82	0.82	120

Table 4.14 shows k-fold cross validation average results on fully connected classifier (NN)

	User accuracy	Producer accuracy	F1-score	Support
Undamaged	0.86	0.93	0.89	82
Damaged	0.82	0.68	0.74	38
Avg/total	0.85	0.85	0.84	120

Considering Figure 4.7, it is clear that there is some high correlation between some methods such as NDVI image difference values and NDREI image difference values.

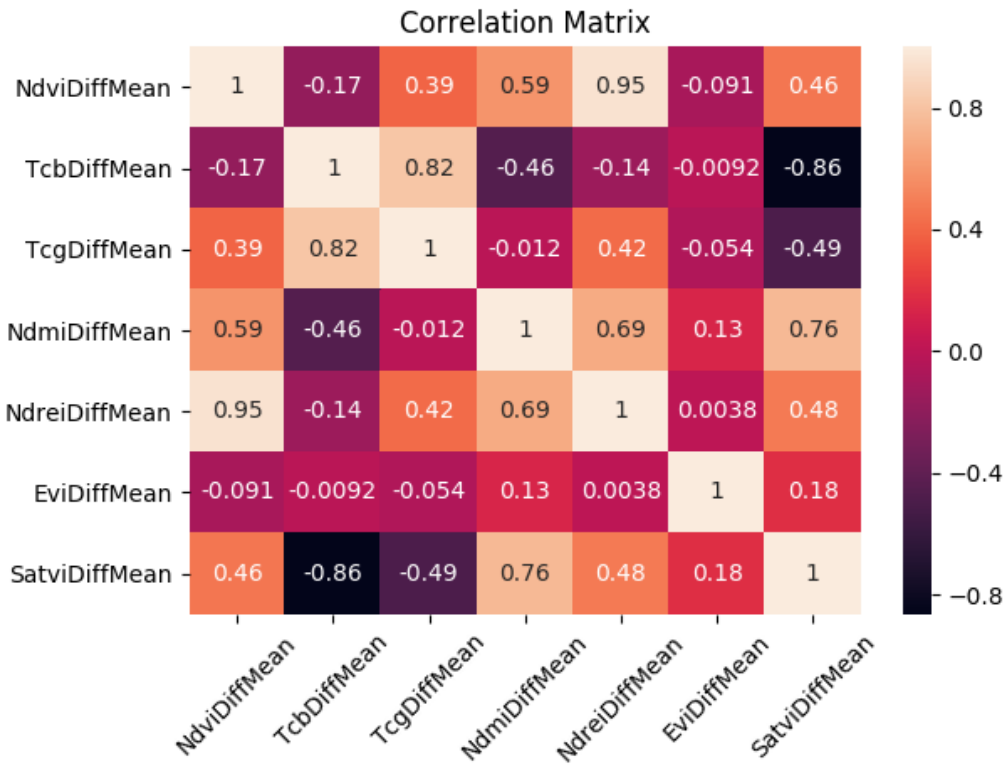

Figure 4.7 shows correlation between different methods used as predictors in the classifiers

In the second dataset, the highest rate of correlation happened between NDVI and NDREI image differences (0.95), which was the same case as the first dataset. TCG and TCB methods also experienced a strong positive correlation, which can be seen from figure 4.7. In addition, SATVI and NDMI image differences saw a positive considerable correlation, which was about 0.76 percent.

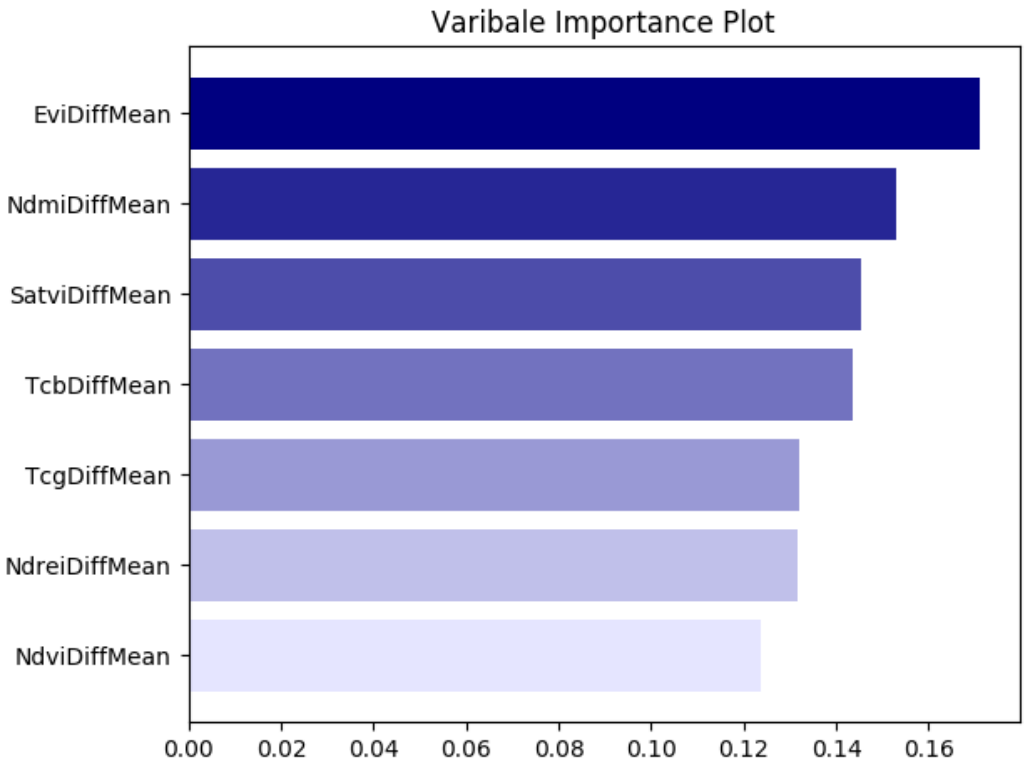

Figure 4.8 variable importance plot achieved in average-based using the second dataset

The most effective predictive methods were EVI, NDMI image differences, followed by SATVI. NDREI and NDVI image differences were the least important variables in the classifiers, which is clear from figure 4.8.

Applying the test dataset on the models, both RF and NN reached user and producer accuracy of 80 percent in average using the balanced test dataset, which is obvious from tables 15 and 17. However, using unbalanced test data, both classifiers managed to reach an average user and producer accuracy of 94 percent, which can be seen from tables 16 and 18.

Table 4.15 shows classification report for RF on the balanced test dataset

	User accuracy	Producer accuracy	F1-score	Support
Undamaged	0.82	0.88	0.85	57
Damaged	0.76	0.67	0.71	33
Avg/total	0.80	0.80	0.80	90

Table 4.16 shows classification report for RF on the unbalanced test dataset

	User accuracy	Producer accuracy	F1-score	Support
Undamaged	0.98	0.95	0.96	100
Damaged	0.55	0.75	0.63	8
Avg/total	0.95	0.94	0.94	108

Table 4.17 shows classification report for NN on the balanced test dataset

	User accuracy	Producer accuracy	F1-score	Support
Undamaged	0.82	0.91	0.86	58
Damaged	0.80	0.62	0.70	32
Avg/total	0.81	0.81	0.80	90

Table 4.18 shows classification report for NN on the unbalanced test dataset

	User accuracy	Producer accuracy	F1-score	Support
Undamaged	0.97	0.97	0.97	100
Damaged	0.62	0.62	0.62	8
Avg/total	0.94	0.94	0.94	108

5. Discussion

Kiira storm that hit South and South East of Finland caused sever damages to the forest in the region on 12th of August 2017. The main goal of this study was to make the process of wind damage detection automated using Sentinel-2 imagery. Univariate image differencing (known as UID) was implemented to extract changed features using six common vegetation indices that enjoyed combination of NIR, RED, SWIR, and BLUE. Two sets of data were used in this study. The first one was created using the whole extent of the images while the other used the subset of the scenes. Considering the results achieved using the first dataset, it is clear that average-based strategy outperformed pixelwise approach, which was about 80 percent user accuracy compared to 70 achieved by pixelwise, which can be seen in tables 4.3 and 4.5. The reason for this improvement could be that by averaging the pixels inside each stand, the effect of cloud noise decreased. The second reason might be that by masking the stands that had less than 80 percent pixel coverage, some of noisy pixels were eliminated from the training data. This might have also removed some healthy pixels from the images. It should be also considered that the ground truth data, forest use notifications created by forest owners, could have had some errors.

Despite all actions taken to cope with the noises, the user accuracy did not go higher than eighty percent as long as the datasets that were formed from the whole extent of the images were used. Considering the achieved user accuracies shown in table 4.1- 4.12, it is clear that the models could not generalize well enough to be considered for a real application because they would make too many false positive and false negative decisions. This issue would get worse when an unbalanced test data was used, meaning that by a user accuracy of about 80 percent, the classifier would fail to differentiate between the classes and ignore the minority class. To show this in practice, unbalanced datasets were inspired and formed manually from the existing test dataset in order to be tested on the models. Looking at the results in tables 4.4, 4.6, 4.10 and 4.12, it is safe to say that both classifiers ignored the minority class (damaged) and voted only for class 0, undamaged, which is obvious from the classification reports where undamaged class received a user accuracy of 1 while the other class saw a zero-user accuracy. The average/total section showed a perfect classification score though, which might be confusing. This is because the classification report was set on weight average mode, which calculated the average accuracy based on the frequency of the

observations used in the classes, meaning that the bigger frequency a class had, the bigger weight it got in the averaging process.
However, considering the second dataset that was generated from the subset of the scenes to be used only in average-based approach, the results were more satisfying because the classifiers could manage to separate the two classes better using balanced and unbalanced test data, which is obvious from their classification reports shown in tables 15-18. As seen, using the balanced test data, the user accuracy remained almost the same as before (about 80 percent in average case), however, on unbalanced dataset, both classifiers performed better. NN managed 62 percent user accuracy on the damaged class while RF reached 55 percent, ending up with weighted average user accuracy of 94 to 95 respectively.
Looking at the correlation matrix throughout the work, there was a strong positive correlation between NDVI and NDREI, TCB and TCG, SATVI and NDMI, meaning that they probably targeted the same feature, therefore, it would have probably been safe if 3 of them (either TCB, TCG, and SATVI or NDMI, NDVI, and TCG) had been removed.
Considering variable importance plots, it is clear that NDMI, SATVI were the only consistent predictors used in both pixelwise and average-based approaches. The reason for this could be the existence of SWIR band that was not in use inside the other methods, which was also suggested by previous studies that focused on wind disturbance detection in forest.

Ground truth data play an important role in accuracy, reliability of the studies. In this study two different ground truth datasets were used, namely forest use notification reported by forest owners and forest stand data came from Forest center. Using forest use notification, it was assumed that in a specified period of time, 45 days after the storm, all land owners were done with their reports about any possible disturbances that might have occurred, which might not have been the case. This means that there was a high possibility of having stands in undamaged class that were actually damaged. In addition, there was no information of severity of damages inside each individual stands. For instance, if the whole extent of stands were damaged or just a slight area inside. It would be really helpful if this information could be accessible.

It was mentioned that one of the strategies taken to address cloud noise was removal of stands that had less than 80 percent pixel coverage from the dataset. This action might have also removed some correct pixels from calculations. In addition, it also reduced the number

of the damaged stands from 432 to128, meaning that much less ground truth data was in hand for training step, which was a critical factor when training a machine learning model. As mentioned above, two different approaches were taken for feeding the models, namely pixelwise and average based. The reason why average based was considered in this study was that both input images were having a poor quality and there were no better options available. This is indeed the limitation of using optical remote sensing and should be taken into account before deciding on using optical imagery for future projects, meaning that for any application in mind, one should make sure that if there are clear images available. The side effect of this issue (cloud noise) considerably affected not only the time spent on pre-processing of the data but also the quality of accuracy achieved in the final results. The lack of clear imagery around natural phenomena such as storm seems logical because storms mostly happen when it is so cloudy. This means that it usually takes few days to be clear (clear sky), which is not appreciated by remote sensing specialists that are looking for immediate imagery before and after storms. One solution to this could be using clear images that are a bit far away from the date on which natural phenomena happens although care should be taken on choosing the images that are away from the day of interest since possible clear cutting and phenology effects can bring uncertainty to studies.

In addition to averaging pixels and removing stands that had less than 80 percent pixel coverage, two other actions were also implemented in different phases of the work to deal with the left-over noises. The first one went for the creation of an extra filter that was generated to decrease the effect of noisy pixels using k-means clustering algorithm and the second one that went for increasing the number of trees (in case of RF) and deep layers as well as neurons (in case of NN). The reason for increasing the layers and trees was for giving more space and memory for transformation of data points such as translations, 2D and 3D projection which is a routine procedure for complex models. The side effect of these actions caused an extra issue, which was about a need for more computing resources such as a strong GPU to handle the calculations, meaning that the fully connected layer established for this study in particular could not be run locally any more. This issue became much worse when the number of training epochs increased, therefore, it was not possible to implement and run the models on CPU locally. It is worth mentioning that the local GPU could not be used since machine learning models are mostly supported by particular NVIDIA GPU hardware that is engineered for such heavy tasks. To solve this issue, CSC's super cluster computers, Taito, was used, A job was initialized through a batch job system and was sent to the super computer for calculations.

For future studies, using NDMI and SATVI that are benefiting from SWIR bands is recommended. For studies that are involved with noisy imagery, simpler models such as regression models that can learn less from training data for the cost of better generalization of future data is also recommended (tradeoff). Using complex model such as NN would be great only when it is exposed to us that distribution data points in training data is similar to distribution of data points in future datasets used for prediction, which is not often the case for remotely sensed data due to a number of reasons such as atmosphere effects, background canopy radiance involved such as soil effects, precipitation, and type of land cover and so on.

Comparing the work done in this thesis and previous works by other researchers, results enjoyed a better spatial resolution due to using Sentinel-2 10-meter images, resulting in a need for more computational resources due to higher quality of pixels. The achieved results in this thesis also conform the sensitivity of NDMI indices as suggested by the other researchers. Addressing clouds were also the critical part of this study. Random forest, chosen by most previous studies as classifier, also performed well in this thesis despite the fact that it required much less computational resources compared to neural network.

6. Conclusion

This thesis focused on establishing machine learning algorithms to map disturbances caused by winds using Sentinel-2 images. Two complex models, namely random forest and neural network were established to perform binary classification on the input data. Two different strategies were taken in this studies, namely pixelwise and average-based. Looking at the results generated by the models in average-based approach, they seemed more reliable and promising. Despite the fact that pixelwise approach is less computationally expensive than average-based technique, average-based is highly recommended especially for cases that there is high percentage of noise in images. Comparing the performance of the two complex classifiers, no considerable improvement was observed in favor of the deep model, fully connected layer (NN). In fact, both models, NN and RF, performed equally throughout this study. Nevertheless, using simpler models such as RF and logistic regression in applications that involve in usage of remotely sensed data seems wiser since distribution of data in training datasets are often different from future datasets that are going to be used for prediction due to a number of reasons that mentioned above, therefore, in order to have a better and more reliable model that is able to generalize unseen data better, simpler models are recommended, which are also easier and faster to implement. UID, PCC, and selective PCA have been some of the most common change extraction algorithms recommended by previous studies. UID was chosen for the purpose of this study since it was much faster and simpler to implement than the others and also less computationally expensive. UID in particular is recommended for the applications that aim to work in real time due to its simplicity and speed. For detection of wind disturbances in forest, usage of vegetation indices was highly recommended by several articles. In particular, indices that took advantage of SWIR and NIR have proved to be more efficient and sensitive to damage detection in forest. In this study, the performance of NDMI and SATVI that were benefiting from SWIR bands proved the fact that indices that benefit from SWIR and NIR could be considered as the first choices when forest damage detection is the main target of future studies.

7. References

Adler-Golden S, Berk A, Bernstein LS, et al. (1998) FLAASH, a MODTRAN4 atmospheric correction package for hyperspectral data retrievals and simulations, Pasadena, California: JPL PUB. pp 1-9.

Ayala-silva, T., & Twumasi, Y. A. (2004). Hurricane Georges and vegetation change in Puetro Rico using AVHRR satellite data. International journal of Remote Sensing 25, 1629-1640. doi:10.1080/01431160310001595037.

Birth, G.S.; McVey, G.R. Measuring the Color of Growing Turf with a Reflectance Spectrophotometer1. Agron. J. 1968, 60, 640-643.

Carlson TN, Ripley DA (1997) On the relation between NDVI, fractional vegetation cover, and leaf area index. Remote Sens Environ 62(3):241-252.

Ceamanos, X., Waske, B., Benediktsson, J.A., Chanussot, J., Fauvel, M., Sveinsson, J.R., 2010. A classifier ensemble based on fusion of support vector machines for classifying hyperspectral data. Int. J. Image Data Fusion 1 (December (4)), 293-307.

Chavez, P. S., & Kwarteng, A. Y. (1989). Extracting spectral contrast in Landsat Thematic Mapper image data using selective principal component analysis. Photogrammetric Engineering and Remote Sensing, 55, 339-348.

Chavez PS Jr (1996) Image-based atmospheric corrections-Revisited and revised. Photogramm Eng Rem S 62(9):1025-1036.

Chen XX, Vogelmann JE, Rollins M et al. (2011) Detecting post-fire burn severity and vegetation recovery using multi temporal remote sensing spectral indices and field-collected composite burn index data in a ponderosa pine forest. International Journal of Remote Sensing 32: 7905-7927. DOI: 10.1080/01431161.2010.524678.

Collins, J. B., & Woodcock, C. E. (1996). An assessment of several linear change detection technique for mapping fores mortality using multitemporal Landsat TM data. Remote Sensing of Environment, 56, 66-77. doi:10.1016/0034-4257(95)00233-2.

Colwell J.E., Weber F.P., (1981), Forest Change Detection, Proc. 15th International Symposium on Remote Sensing of Environment, Ann Arbor.

Colwell J.E., Weber F.P., (1981), Forest Change Detection, Proc. 15th International Symposium on Remote Sensing of Environment, Ann Arbor.

Congalton, R.G.; Green, K. Assessing the Accuracy of Remotely Sensed Data: Principles and Practices, 2nd ed.; CRC Press Boca Raton, FL, USA, 2009.

Coppin, P., Jonckheere, I., Nackaerts, K., Muys, B., & Lambin, E. (2004). Digital change detection methods in ecosystem monitoring: A review. International Journal of Remote Sensing, 25, 1565-1596. doi:10.1080/0143116031000101675.

Coppin, P., Jonckheere, I., Nackaerts, K., Muys, B., & Lambin, E. (2004). Digital change detection methods in ecosystem monitoring: A review. International Journal of Remote Sensing, 25, 1565-1596. doi:10.1080/0143116031000101675.

Coppin, P. R., & Bauer, M. E. (1994). Processing of multitemporal Landsat TM imagery to optimize extraction of forest cover change features. IEEE Transactions on Geoscience and Remote Sensing, 32, 918-927. foi:10.1109/36.298020.

Crist, E. P., Laurin, R., & Cicone, R. C. (1986). Vegetation and soils information contained in transformed Thematic Mapper data. Proceedings of International Geosciences and Remote Sensing Symposium (IGRASS) 86 Symposium. ESA Publications Division, ESA SP-254, European Space Agency, Paris, 1465-70.

Davies, K.p; Murphy, R.J.; Bruce, E. Detecting historical changes to vegetation in a Cambodian protected area using the Landsat TM and ETM+ sensors. Remote Sens. Environ. 2016, 187, 332-344.

De Abelleyra, D.; Veron, S.R. Comparison of different BRDF correction methods to generate daily normalized MODIS 250m time series. Remote Sens. Environ. 2014, 140, 46-59.

Dixon RK, Brow S, Houghton RA et al. (1994) Caron Pools and Flux of Global Forest Ecosystems. Science 263: 185-190. DOI: 10.1126/science.263.5144.185.

Dobson, J.E.; Bright, E.A; Ferguson, R.L.; Field, D.W.; Wood, L.; Haddad, K.D; Iredale III, H.; JENSEN, J.R.; Klemas, V.V.; Orth, J.R.; et al. NOAA Coastal Change Analysis Program (C-CAP): Guidance for Regional Implementation. NOAA Technical Report NMFS 123: Seattle, WA, USA, 1995.

Einzmann, K et al. (2017). Windthrow detection in European forests with high-resolution optical data. DOI: 10.3390 / f8010021.

Eshleman KN, McNeil BE, Townsend PA (2009) Validation of a remote sensing based index of forest disturbance using stream water nitrogen data. Ecological Indicators 9: 476-484. DOI: 10.1016/j.ecolined.2008.07.005.

Francois Chollet. (2018) Deep learning with python. United States of America. Manning Publication. 361 p. ISBN 9781617294433.

Franklin, S. E., Moskal, L. M., Lavigne, M.B., & Pugh, k. (2000). Interpretation and classification of partially harvested forest stands in the Fundy model forest using multitemporal Landsat TM digital data. Canadian Journal of Remote Sensing, 26, 318-333.

Fugui Wang., & Y.Jun Xu. (2009). Comparison of remote sensing change detection techniques for assessing hurricane damage to forests.

Gislason, P.O., Benediktsoon, J.A., Sveinsson, J.R., 2006. Random Forests for land cover classification. Pattern Recognit. Lett. 27 (no. 4), 294-300.

Giuseppe Bonaccorso. (2018) Machine learning algorithms. United Kingdom. Packt Publishing Ltd. 522 p. ISBN 979-1-78934-799-9.

Griffiths P, Kuemmerle T, Baumann M, et al. (2013) Forest disturbances, forest recovery, and changes in forest types across the Carpathian ecoregion from 1985 to 2010 based on Landsat image composites. Remote Sensing of Environment. DOI: 10.1016/j.rse.2013.04.022.

Griffiths, P.; Kuemmerle, T.; Baumann, M.; Radeloff, V.C.; Abrudan, I.V.; Lieskovsky, J.; Munteanu, C.; Ostapowicz, K.; Hostert, P. Forest disturbances, forest recovery, and changes in forest types acress the Carpathian ecoregion from 1985 to 2010 based on Landsat image composites. Remote Sens. Environ. 2014, 151, 72-88.

Grifiths, P.; Kuemmerle, T.; Kennedy, R.E.; Abrudan, I.V.; Knorn, J.; Hostert, P. Using annual time-seris of Landsat images to assess the effects of forest restitution in post-socialist Romania. Remote Sens. Environ. 2012, 118, 199-214.

Guo XY, Zhang HY, Wang YQ, et al. (2015) Mapping and assessing typhoon-induced forest disturbance in Changbai Mountain National Nature Reserve using time series Landsat imagery. Journal of Mountain Science 12(2). DOI: 10.1007/s11629-014-3206-y.

Gutman G, Ignatov A (1998) The derivation of the green vegetation fraction from NOAA/AVHRR data for use in numerical weather prediction models. Int J Remote Sens 19(8):1533-1543.

Hadi & Rautiainen. Monitoring Deforestation in rainforest using satellite data. 2018. Vol 26.

Hais, M.; Wild, J.; Berec, L.; Bruna, J.; Kennedy, R.; Braaten, J.; Broz, Z. Landsat imagery spectral trajectories-important variables for spatially predicting the risks of bark beetle disturbance. Remote Sens. 2016, 8, 687.

Hansen, M. J., Franklin, S. E., Woudsma, C., & Peterson, M. (2001). Forest structure classification in the North Columbia Mountains using the Landsat TM Tasseled Cap wetness component. Canadian Journal of Remote Sensing, 27, 20-32.

Hegaret-Mascle, S. L., Seltz, R., Hubert-Moy, L., Corgne,S., & Stach, N. (2006). Performance of change detection using remotely sensed data and evidential fusion: Comparison of three cases of application. International Journal of Remote Sensing, 27, 3515-3532. doi:10.1080/01731160500300255.

Hobbs RJ, Huenneke LF (1992) Disturbance, diversity, and invasion: implications for conservation. Conservation Biology 6:324-337. DOI: 10.1046/j.1523-1739.1992.06030324.x.

Horler, D. N. H., & Ahern, F. J. (1986). Forestry information-content of Thematic Mapper data. International Journal of Remote Sensing, 7, 405-428. doi:10.1080/01431168608954695.

Huete, A., Justice, C., & Liu, H. (1994). Development of vegetation and soil indices fore MODIS-EOS. Remote Sensing of Environment, 25, 295-309. doi:10.1016/0034-4257(88)90106-X.

Huete, A. R., Liu, H., & van Leeuwen, W.J. D. (1997a). The use of vegetation indices in forested regions: Issues of linearity and saturation. Geoscience and Remote Sensing, 1997. IGARSS 97. Remote sensing a scientific vision for sustainable development, 1997 IEEE International, 1966-1968.

Iacobescu O., Barnoaiea I., Bofu C., (2012), An up-to-date land degradation inventory in Suceava Plateau using digital orthophotographs, Environmental Engineering and Management Journal, 11, 1667-1677.

Iordache E., (2001), Effects of opening conifer stands by skid roads to growth and yield, Annals of Forest Research, 1, 92-95.

Jensen, J. Remote Sensing of the Environment: An Earth Resource Perspective; University of Minnesota, Pearson Prentice Hall: Upper Saddle River, NJ, USA, 2007; p.592, ISBN 0131889508.

Ji, L., & Peters, A. J. (2007). Performance evaluation of spectral vegetation indices using a statistical sensitivity function. Remote Sensing of Environment, 106, 59-65. doi:10.1016/j.rse.2006.07010.

Jiang Z, Huete AR, Chen J, Chen Y, Li J, Yan G, Zhang X (2006) Analysis of NDVI and scaled difference vegetation index retrievals of vegetation fraction. Remote Sens Environ 101(3):366-378.

Jin, S.; Sader, S.A. Comparison of time series tasseled cap wetness and the normalized difference moisture index in detecting forest disturbances. Remote Sens. Environ. 2005, 94, 364-372.

Kaufmann R.K., Seto K.C., (2001), Change detection, accuracy, and bias in a sequential analysis of Landsat imagery in the Pearl River Delta, China: econometric techniques, Agriculture, Ecosystems and Environment 85, 95-105.

Kwarteng, A. Y., & Chavez, P. S. (1998). Change detection study of Kuwait City and environs using multi-temporal Landsat Thematic Mapper data. International Journal of Remote Sensing, 19, 1651-1662. doi:10.1080/014311698215162.

Linden SVD, Janz A, Waske B, Eiden M, Hostert P (2007) Classifying segmented Hyperspectral data from a heterogeneous urban environment using support vector machines. J Appl Remote Sens 1(1):341-353.

Liu Y.G., Wang N.L., Wang L.G., Zhao Y.Q., BoWu X. (2013), Application of GIS in regional ecological risk assessment of water resources, Environmental Engineering and management Journal, 12, 1465-1474.

Lyon, J. G., Yuan, D., Lunetta, R. S., & Elvidge, C. D. (1998). A change detection experiment using vegetation indices. Photogrammetric Engineering and Remote Sensing, 64, 143-150.

Marsett, Robert, et al. Remote Sensing for Grassland Management in the AridSoutwest, vol. 59, no 5, 2006, doi:10.2458/azu_jrm_v59i5_marsett.

Melendez-Pastor I., Navarro-Pereno J., Koch M., Gomez I., Hernandez E.I., (2013), Evaluation of land degradation after forest fire using a fuzzy logic model, Environmental Enginering and Management Journal, 12, 2087-2096.

Mountrakis G, Im J, Ogole C (2011) Support vector machines in remote sensing: a review. ISPRS J Photogramm 66:247-259.

Nackaerts, K., Vaesen, K., Muys, B., & Coppin, P. (2005). Comparative performance of a modified change vector analysis in forest change detection. International Journal of Remote Sensing, 26, 839-852. doi:10.1080/0143116032000160462.

Nita M.D., Clinciu I., (2010), Hyidrological mapping of the vegetation using remote sensing products, Buttetin of the Transilvania University of Brasov, 52, 73-79.

Oguz H., (2013), LST calculator: a program for retrieving land surface temperature from Landsat TM/ETM+ imagery, Environmental Engineering and Management Journal, 12, 549-555.

Paulina Lyubenova Raeva, Jaroslav Sedina, Adam Dlesk., 2018. Monitoring of crop fields using multispectral and thermal imagery from UAV.

Pflugmacher, D.; Cohen, W.B; Kennedy, R.E. Using Landsat-derived disturbance history (1972-2010) to predict current forest structure. Remote Sens. Environ. 2012, 122, 146-165.

Ramsey, E. W., Chappell, D. K., & Baldwin, D. G. (1997). AVHRR imagery used to identify hurricane damage in a forested wetland of Louisiana. Photogrammetric Engineering and Remote Sensing, 63, 293-297.

Ramsey, E. W., Hodgson, M. E., Sapkota, S. K., & Nelson, G. A. (2001). Forest impact estimated with NOAA AVHRR and Landsat TM data related to an empirical hurricane wind-field distribution. Remote Sensing of Environment, 77, 279-292. doi:10.1016/S0034-4257(01)00217-6.

Rouse, J.W.; Hass, R.H.; Schell, J.A.; Deering, D.W. Monitoring vegetation systems in the Great Plains with ERTS. In Proceedings of the Third ERTS Symposium NASA, Washington, DC, USA, 10-14 December 1973; Volume 1, pp. 309-317.

Schneider A (2012) Monitoring land cover change in urban and peri-urban areas using dense time stacks of Landsat satellite data and a data mining approach. Remote Sens Environ 124:689-704.

Schultz, M.; Clevers, j.G.P.W.; Carter, S.; Verbesselt, j.; Avitabile, V.; Quang, H.V; Herold, M. Performance of vegetation indices from Landsat time series in deforestation monitoring. Int. J. Appl. Earth Obs. Geoinf. 2016, 52, 318-327.

Shao GF, Shugart HH, Zhao G, et al. (1996) Forest cover types derived from Landsat Thematic Mapper imagery fore Changbai Mountain area of China. Canadian Journal of Forest Research 26: 206-216. DOI: 10.1139/x26-024.

Song, C.; Woodcock, C.E.; Seto, K.C.; Lenney, M.P.; macomber, S.A. Classification and change detection using Landsat TM data: When and how to correct atmospheric effects? Remote Sens. Environ. 2001, 75, 230-244.

Stych, P.; Lastovicka, J.; Hladky, R; Paluba. Evaluation of the influence of disturbances on forest vegetation using the time series of Landsat Data (2019).

Tao J, Zhang Y, Yuan X, et al. (2013) Analysis of forest fires in Northeast China from 2003 to 2011. International Journal of Remote Sensing 34: 8235-8251. DOI: 10.1080/01431161.2013.837229.

Tigges J, Lakes T, Hostert P (2013) Urban vegetation classification: benefits of multi temporal RapidEye satellite data. Remote Sens Environ 136(5):66-75.

Torbick, Nathan, et al. Regional Mapping of Plantation Extent Using Multisensor Imagery. Remothe Sensing, vol. 8, no. 12, 2016, p. 236., doi:10.3390/rs8030236.

Van doninck, J.: Tuomisto, H. Evaluation of drectional normalization methods for Landsat TM/ETM+ over primary Amazonation lowland forests. Int. J. Appl. Earth Obs. Geoinf. 2017, 58, 249-263.

Vogelmann, J.E; Xian, G.; Homer, C.; Tolk, b. Monitoring gradual ecosystem change using Landsat time series analyses: Case studies in selected forest and rangeland ecosystems. Remote Sens. Environ. 2012, 122, 92-105.

Vorovencii, L. (2014) Detection of environmental changes due to windthrows using Landsat-7 ETM+ satellite images. DOI: 10.30638/eemj.2014.060.

Wang, J.; Sammis, T.W.; Gutshick, V.P; Gebremichael, M.; Dennis, S.O.; Harrison, R.E. Revies of Satellite Remote Sensing Use in Forest Health Studies. Open Geogr. J. 2010, 3, 28-42.

Wang M, Xu H. (2018) Remote sensing-based assessment of vegetation damage by a strong typhoon (Meranti) in Xiamen Island, China. Nat Hazards (2018) 93:1231-1249.

Wear, D.N., & Greis, J.G. (2002). Southern forest resource assessment. USDA Forest Service, Southern Research Station, Gen. Tech. Rep. SRS-54.

Xu HQ, He H, Huang SL (2013) Analysis of fractional vegetation cover change and its impact on thermal environment in the Hetian basinal area of County Changting, Fujian province, China (in Chinese). Acta Ecol Sin 33(10):2954-2963.

Xue, Jinru, and Baofeng Su., 2017. Significant Remote Sensing Vegetation Indices. Pp. 17., doi: 10.1155/2017/1353691.

Zhang, H.K.; Roy, D.P; Yan, L; Li, Z; Huang, H.; Vermote, E.; Skakun, S.; Roger, J.C. Characterization of Sentinel-2A and Landsat-8 top of atmosphere, surface, and nadir BRDF adjusted reflectance and NDVI differences. Remote Sens. Environ. 2018, 215, 482-494.

Links

1)Yle Uutiset (2017),Saturday night storm downs trees, cuts electricity in the south, Yle Uutiset,viewed102.03.2019,https://yle.fi/uutiset/osasto/news/saturday_night_storm_downs_trees_cuts_electricity_in_the_south/9773250.

2)Yle Uutiset(2016), Electricity companies race to restore power to 75,000 homes, Yle Uutiset, viewed 02,03,2019 https://yle.fi/uutiset/osasto/news/electricity_companies_race_to_restore_power_to_75000_homes/9125883.

3)Bretch(2018),Remote Sensing Indices, medium corporation (US),viewed 01.02.2019, https://medium.com/regen-network/remote-sensing-indices-389153e3d947.

4) aineistot.metsaan, aineistot.metsaan.fi.avoinmetsatieto.Metsankayttoilmoitukset.Maakunta, https://aineistot.metsaan.fi/avoinmetsatieto/Metsankayttoilmoitukset/Maakunta/, 14.01.2019

5)metsakeskus, forestusedeclaration,viewed 14.01.2019, https://www.metsaan.fi/sites/default/files/avoin-metsatieto-mki-tietokantakaavio.pdf.

6) metsakeskus, avoin-metsatieto-koodisto_0-4, viewed 14.1.2019 https://www.metsaan.fi/sites/default/files/avoin-metsatieto-koodisto_0.xlsx.

7)Metsakeskus, forest stand features,viewed 14.01.2019, https://www.metsaan.fi/sites/default/files/avoin-metsatieto-kuviot-tietokantakaavio.pdf.

8) metsakeskus, metsatietostandardienSanomakuvauksetkoodistot_v13-5, viewed 14.1.2019, https://extra.bitcomp.fi/metsastandardidata/erilliskokonaisuudet/sanomaexcelit/MetsatietostandardienSanomakuvauksetKoodistot_V13.xlsx

9)Metsakeskus, forest stand features,viewed 14.01.2019, https://www.metsaan.fi/sites/default/files/avoin-metsatieto-kuviot-tietokantakaavio.pdf.

10) esa Copernicus, Copernicus Open Access Hub, viewed 08.12.2018 https://scihub.copernicus.eu/dhus/#/home.

11)CSC, Non-forest mask, viewed 11,01.2019, wrk/project_ogiir-csc/luke/2015/maaluokka_vmi1x_1216.img.

12) Kai Makisara, Matti Katila ,Jouni Perasaari(2019), The Multi-Source National Forest Inventory of Finland - methods and results 2015, Natural Resources Institute Finland, Helsinki, viewed 01.01.2019,]http://jukuri.luke.fi/bitstream/handle/10024/543826/luke-luobio_8_2019.pdf?sequence=6&isAllowed=y

13) Mäkisara, Kai; Katila, Matti; Peräsaari, Jouni (2019), The Multi-Source National Forest Inventory of Finland – methods and results 2015,04.26.12.1018, http://jukuri.luke.fi/handle/10024/543826.

14) UltrahackHackathon (2018), Data descriptionsfor Open ForestData Sets,metsakeskus,viewed 02.01.2019, https://www.metsakeskus.fi/sites/default/files/ultrahack/open_forest_data_descriptions_for_hackathon.pptx.pdf.

15) metsatietostandard(2014), FOREST USE DECLARATIONS, metsatieostandard esittelysivusto, viewed 10.02.2019, https://www.metsatietostandardit.fi/en/standards/forest-use-declarations/.

16) Ministry of Agriculture and Forestry(1996),forest act, Ministry of Agriculture and Forestry, Finland,viewed 10.01.2019, https://www.finlex.fi/fi/laki/kaannokset/1996/en19961093_20140567.pdf.

17)senitel online, Level-2A Algorithm Overview,viewd 01.02.2019, https://earth.esa.int/web/sentinel/technical-guides/sentinel-2-msi/level-2a/algorithm.

18)Metsakeskus(2017),Paikkatietoaineistot,Metsakeskus,viewed 10.01.2019

https://www.metsaan.fi/paikkatietoaineistot.